ELSEVIER

Contents lists available at ScienceDirect

Applied Energy

journal homepage: www.elsevier.com/locate/apenergy





Planning-Oriented resilience assessment and enhancement of integrated electricity-gas system considering multi-type natural disasters

Han Wang ^{a,b}, Kai Hou ^{a,*}, Junbo Zhao ^c, Xiaodan Yu ^a, Hongjie Jia ^a, Yunfei Mu ^a

- ^a Key Laboratory of Smart Grid of Ministry of Education, Tianjin University, Nankai District, Tianjin 300072, China
- ^b State Grid Zhengzhou Electric Power Supply Company, Zhengzhou 450000, China
- ^c The Department of Electrical and Computer Engineering, University of Connecticut, Storrs, CT 06269, USA

HIGHLIGHTS

- A framework is proposed to describe the generic natural disaster modelling process.
- The disaster scenario database is constructed to provide data for resilience research.
- Reusable impact-increment database is built to accelerate resilience assessment.
- Component-level indices are proposed for targeted resilience enhancement.

ARTICLE INFO

Keywords: Resilience Assessment Resilience Enhancement Integrated Electricity-Gas System Multi-type Natural Disasters Reusable Impact-Increment Database

ABSTRACT

A planning-oriented resilience assessment and enhancement approach is proposed that can efficiently deal with multi-type natural disasters. A unified disaster modelling framework is proposed to extract key information from various potential disaster scenarios, thus forming a disaster scenario database. The impact-increment-based enumeration method is applied, and a reusable impact-increment database is established to speed up the assessment process. The reusable database is also utilized to calculate component-level resilience indices and economic indices, so as to make enhancement strategies against potential disasters within planning time scale. Resilience assessment on an integrated electricity-gas system in Taiwan's coastal seismic statistical zone shows that the proposed method can significantly improve the computational efficiency as compared to existing methods. Numerical results indicate that the resilient planning considering the diversity of natural disaster types comprehensively improves the system resilience, which means it is not only concerned with the system performance under a single type of disaster. In addition, the most suitable resilience enhancement scheme with insufficient funds shall be developed according to the economic indices, instead of the component-level resilience indices that cannot balance the resilience enhancement effect with the implementation cost.

1. Introduction

Affected by climate changes, extreme events, such as natural disasters have become more and more frequent, which threatens the normal operation of the integrated electricity-gas system (IEGS). In 2011, the Great East Japan Earthquake caused blackouts and multiple gas pipeline rupture accidents [1,2]. In 2013, Super Typhoon Usagi landed in Guangdong Province, causing one 500 kV line and six 220 kV lines to be out of service [3]. IEGS is prone to high-order faults under natural disasters, which often lead to electricity and gas shortages. For

this reason, the concept of resilience has been used to assess the ability of the existing or planned system to withstand disasters and quickly return to normal operating conditions [4–6].

Many studies have been carried out on resilience indices. It is well known that the resilience includes four factors: robustness, redundancy, resourcefulness, and rapidity [7,8]. Among them, redundancy and resourcefulness describe the means of improving resilience, while the corresponding effect is measured by robustness and rapidity [9]. The resilience triangle [9] and the resilience trapezoid [10] describe the resilience index in terms of robustness and rapidity, which can reflect the common influence of the four factors. Furthermore, the planning-

 $\textit{E-mail addresses:} \ \, \text{hanw19@tju.edu.cn} \ \, \text{(H. Wang), khou@tju.edu.cn} \ \, \text{(K. Hou), junbo@ece.msstate.edu} \ \, \text{(J. Zhao), yuxd@tju.edu.cn} \ \, \text{(X. Yu), hjjia@tju.edu.cn} \ \, \text{(H. Jia), yunfeimu@tju.edu.cn} \ \, \text{(Y. Mu).}$

 $^{^{\}star}$ Corresponding author.

Abbreviations EGS Integrated electricity-gas system Part	Nomenc	lature	$d\theta$, dH , dv	ν the segment intervals of the feasible regions of θ , ΔH_0 and
Integrated electricity-gas system	Abbrevia	tions	¢	v_T respectively
EPS electrical power system $V_{a/b}$ design wind speed of the transmission line segment MCS monte carlo simulation Δh length of the transmission line segment MCS state enumeration Δh length of the transmission line segment ISE impact-increment-based state enumeration ΔL ΔL the calculation time of RD using ISE-R3 method OPF optimal power flow Voriables between the calculation time of RD using ISE-R3 method DSD disserter senario database $E[Q_{And}]$ the calculation time of RD using MCS-R method OPA disserter probability model $E[Q_{And}]$ the calculation time of RD using MCS-R method CE combhanterial enumeration Q_{and} the calculation time of RD using MCS-R method CE combhanterial enumeration Q_{and} the calculation time of RD using MCS-R method DAM disaster probability model Q_{and} the calculation time of RD using MCS-R method CE combhanterial enumeration Q_{and} the calculation time of RD using MCS-R method CE combhanterial enumeration Q_{and} the deliver			5	e e e e e e e e e e e e e e e e e e e
NSS moter carlo simulation Δh is state enumeration Δh in the carlo simulation Δh in the carlo simulation Δh is state enumeration Δh in the carlo of the transmission line segment during typhone $a_1 = b_1 + b_2 + b_3 + b_4 + b_4 + b_4 + b_5 + b_5 + b_6 + $			$v_{d.tw}$	design wind speed of the transmission tower
MCS so monte carlo simulation $Δt$ interval of the transmission line segment $Λt$ interval of the time segment arriving typhono and $Λt$ interval of the time segment arriving typhono $Λt$ interval of the time segment of the calculation time of RD using ISS-R3 method the calculation time of RD using ISS-R3 method $Λt$ interval of the time segment of the calculation time of RD using ISS-R3 method $Λt$ interval of the time segment of the calculation time of RD using ISS-R3 method $Λt$ interval of the time segment of the calculation time of RD using ISS-R3 method $Λt$ interval of the time segment $Λt$ interval of the calculation time of RD using ISS-R3 method the calculation time of RD u	NGS	natural gas system		design wind speed of the transmission line segment
Insert Increment-based state enumeration Times	MCS	monte carlo simulation		length of the transmission line segment
RO robust optimization T_{KES} the calculation time of RD using MCS-R method DSD disaster secarato database Variables DPM disaster probability model F_{CASC} CE combinatorial enumeration Q_{obst} BSR background source region I_{c} BSR background source region I_{c} FGA peak ground velocity the initial load loss of IEGS caused by fault state of the probability of component I_{c} FGD peak ground displacement I_{c} Cov coefficient of variance P_{c} FGD peak ground displacement I_{c} Cov coefficient of variance P_{c} Indices and sets I_{c} Indices of component in IEGS I_{c} I index of component in IEGS I_{c} I index of overhead transmission line I_{c}	SE	state enumeration	Δt	interval of the time segment during typhoon
$ \begin{array}{c ccccccccccccccccccccccccccccccccccc$	IISE		T_{IISE}	the calculation time of RD using IISE-R3 method
DSD disaster scaratio database $ Variabhse E Q_{lood} $ the expected load shedding of IEGS $ Variabhse $ the expected load shedding of IEGS $ Variabhse $ the expected load shedding of IEGS $ Variabhse $ the expected load shedding of IEGS $ Variabhse $ the expected load shedding of IEGS $ Variabhse $ the expected load shedding of IEGS $ Variabhse $ the expected load shedding $ Variabhse $ the expected load shedding of IEGS $ Variabhse $ the expected load shedding of IEGS $ Variabhse $ the expected load shedding $ Variabhse $ the expected load shedding $ Variabhse $ the expected load shedding of IEGS $ Variabhse $ the expected load shedding $ Variabhse $ the expected load shedding $ Variabhse $ the expected load shedding of IEGS component $ Variabhse $ the expected load shedding $ Variabhse $ the expected load shedding $ Variabhse $ the efailure probability of component $ Variabhse $ the efailure probability of component $ Variabhse $ the efailure probability of component $ Variabhse $			T_{MCS}	the calculation time of <i>RD</i> using MCS-R method
DNM disaster probability model P_{abat} disaster probability model P_{abat} the expected load shedding of IEGS the electric load shedding of IEGS the electric load shedding of IEGS and some and the expected load shedding of IEGS and some and the electric load shedding of IEGS and some and the electric load shedding of IEGS and some and the electric load shedding of IEGS and some and the electric load shedding of IEGS and some and the electric load shedding of IEGS and some and the electric load shedding of IEGS and some and the electric load shedding of IEGS and some and the electric load shedding of IEGS and some and the electric load shedding of IEGS and some and the electric load shedding of IEGS and some and the electric load shedding of IEGS and some and the electric load shedding of IEGS and the electric load shedding of IEGS and some and the electric load shedding of IEGS and some and the electric load shedding of IEGS and the electric load shedding of IEGS and the electric load shedding of IEGS and the elimitation and the elimital load loss of IEGS caused by fault state in the initial load loss of IEGS caused by fault state in the initial load loss of IEGS caused by fault state in the initial load loss of IEGS caused by fault state in the initial load loss of IEGS caused by fault state in the initial load loss of IEGS caused by fault state in the initial load loss of IEGS caused by fault state in the initial load loss of IEGS caused by fault state in the initial load loss of IEGS caused by fault state in the initial load loss of IEGS caused by fault state in the initial load loss of IEGS caused by fault state in the initial load loss of IEGS caused by fault state in the initial load loss of I			Variables	
DAM disaster attack model Q_{bad} combinatorial enumeration Q_{bad} the gas load shedding the gas load shedding Q_{bad} the failure probability of component n the initial load loss of IEGS caused by fault state S_{bad} the failure probability of component n the initial load loss of IEGS caused by fault state S_{bad} the failure probability of component n the initial load loss of IEGS caused by fault state S_{bad} the failure probability of component n the section of the failure probability of seen and S_{bad} the failure probability of seen and S_{bad} the failure probability of seen and S_{bad} the failure probability of component n under disaster seen S_{bad} the failure probability of component n under disaster seen S_{bad} the failure probability of component n under disaster seen S_{bad} the failure probability of component n under disaster seen S_{bad} the failure probability of component n under disaster seen S_{bad} the failure probability of component n under disaster seen S_{bad} the failure probability of component n under disaster seen S_{bad} the failure probability of component n under disaster seen S_{bad} the failure probability of component n under disaster seen S_{bad} the failure probability of component n under disaster seen S_{bad} the failure probability of component n under disaster seen S_{bad} the failure probability of component n under disaster seen S_{bad} the failure probability of component n under disaster seen S_{bad} the failure probability of component n under disaster seen S_{bad} the failure probability of component n under disaster seen S_{bad} the set of potential disaster seen S_{bad} the failure probability of each basic disaster parameter S_{bad} the set of potential disaster seen S_{bad} the failure probability of each basic disaster parameter S_{bad} the set of potential disaster s				the expected load shedding of IEGS
CE combinatorial enumeration P_{t} background source region P_{t} background source region P_{t} background source region P_{t} be failure probability of component P_{t} the initial load loss of IEGS caused by fault state flower P_{t} be ground velocity P_{t} be ground veloci		•		
BSR background source region Fig. 1 BSR background source region Fig. 1 BSR background source region Fig. 2 Fig. 2 Fig. 3 Fig. 4 Fi				· · · · · · · · · · · · · · · · · · ·
TSR tectonic source region PGA peak ground acceleration PGV peak ground decolity PGD peak ground displacement PGV peak ground displacement in IEGS PGV peak ground displacement PGV peak ground displacement PGV peak ground displacement in IEGS PGV peak ground displacement PGV peak ground displace				
PGA peak ground acceleration d_i the fimpact-increment of fault state s of the potential disaster secaration TD peak ground velocity p peak ground displacement p the scenario weight of d_i the scenario weight of d_i the failure probability of component in IEGS p index of component in IEGS p index of component in IEGS p index of disaster type q index of transformer p index of overhead transmission line p index of overhead transmission line p index of overhead transmission tower p index of power transmission tower p index of power transmission line segment p in the set of p or porter fault states p in the set of p or porter fault states p in the set of p or porter fault states p in the set of p or porter fault states p in the set of p or porter fault states p in the set of p or porter fault states p in the set of p or porter fault states p in the set of p or porter fault states p in the set of p or porter fault states p in the set of p or porter fault states p in the set of p or porter fault states p in the set of p or porter fault states p in the set of p or porter fault states p in the set of p or porter fault states p in the set of p or porter fault states p in the set of p or porter fault states p in the			I_s	the initial load loss of IEGS caused by fault state s
PGD peak ground displacement w_i the esth potential disaster scenario in TD to coefficient of variance TD peak ground displacement TD peak ground gro		<u> </u>	ΔI_{s}	the impact-increment of fault state s
The courrence probability of scenario d_i the failure probability of scenario d_i and index of component in IEGS In index of component in IEGS Index of transformer ω index of transformer ω index of power transmission line i index of power transmission line i index of power transmission line index of gas pipeline i index of power transmission line index of gas pipeline segment i index of gas pipeline segment i index of power transmission line segment i index of gas pipeline i ind			d_i	•
the failure probability group of IEGS component in IEGS $p_{l.n}$ the failure probability of component n under disaster scenario d_l index of disaster type n index of component in IEGS n index of transformer n index of transformer n index of overhead transmission line n index of power transmission line n index of power transmission line segment n index of gas pipeline segment n index of power transmission line segment n index of power limit of earthquake magnitude segment n index of power limit of earthquake magnitude n in the set of position of the power limit of earthquake magnitude n in the earthquake magnitude	PGD	peak ground displacement		ğ -
$ \begin{array}{c c c c c c c c c c c c c c c c c c c $	Cov	coefficient of variance		- · · · · · · · · · · · · · · · · · · ·
$ \begin{array}{cccccccccccccccccccccccccccccccccccc$	Indian	nd cate	F_i	
$ \begin{array}{c} I & \text{index of transformer} \\ $			n.	-
ω index of transformer $ω$ index of overhead transmission line $ρ$ index of gas pipeline $ρ$ index of gas pipeline $ρ$ index of gas pipeline $ρ$ index of gower transmission tower $ρ$ index of gower transmission line segment $ρ$ index of gower transmission line segment $ρ$ index of gower transmission line segment $ρ$ index of gas pipeline $ρ$ index of gas pipeline $ρ$ index of gas pipeline $ρ$ in the set of potential disaster scenarios $ρ$ in the set of potential Type- l disaster scenarios $ρ$ in the set of potential Type- l disaster scenarios $ρ$ in the set of potential disaster scenarios $ρ$ in the set of potential disaster scenarios $ρ$ in the set of potential disaster scenarios $ρ$ in the set of failed components $ρ$ in the set of fon-failed components $ρ$ in the set of fon-failed components $ρ$ in the set of inner gain to overhead transmission line $ρ$ in the set of line segments belonging to overhead transmission line $ρ$ in the set of pipeline segments belonging to overhead transmission line $ρ$ in the set of pipeline segments belonging to gas pipeline $ρ$ in the failure probability of transmission line segments and constants $ρ$ in the low calorific value of natural gas $ρ$ in the low calorific value of natural gas $ρ$ in the cardinality of fault state $ρ$ in the cardinality of $ρ$ fall the cardinality of $ρ$ for the animal frequency of Type- l disaster $ρ$ in the cardinality of $ρ$ fall the cardinality of $ρ$ for the cardinality of $ρ$ for the cardinality of $ρ$ for the animal frequency of Type- l disaster $ρ$ for the cardinality of $ρ$ for t			Pi.n	
index of overhead transmission line ρ index of gas pipeline ρ index of gas pipeline ρ index of power transmission tower ρ index of power transmission line segment ρ index of gas pipeline ρ index of out of gas pipeline ρ index of gas pipe		7.1	R	-
$ \begin{array}{cccccccccccccccccccccccccccccccccccc$				
h index of power transmission tower h index of power transmission line segment g index of gas pipeline segment g index of gas pipeline segment he set of j-order fault states he set of potential disaster scenarios from the set of failed components from the set of former in the set of potential disaster scenarios from the set of potential disaster scenarios from the set of failed components from the set of former system the set of failure probability of transmission line ω from the set of failure probability of transmission line segment from the failure probability of transmission the failure probability of or overhead transmission from the failure probability of transformer γ the f				
$ \begin{array}{cccccccccccccccccccccccccccccccccccc$				
s fault state denoted by the set of failure components H_n the strongthening cost for component n $Ω_i^k$ the set of j -order fault states M earthquake magnitude $Ω_i^k$ the set of potential disaster scenarios I earthquake intensity D_i the set of potential Type- l disaster scenarios M_j midpoint of the j th earthquake magnitude segm RD the set of potential Type- l disaster scenarios M_j midpoint of the j th earthquake magnitude segm RD the set of potential Type- l disaster scenarios P_i the probability of each basic disaster parameter $\{n \in s\}$ the set of non-failed components p_i the probability of each basic disaster parameter $\{n \in s\}$ the set of foundary alian duration of the p -th earthquake magnitude segm p_i the probability of each basic disaster parameter $\{n \in s\}$ the set of non-failed components p_i the probability of the outer boundary of intens $\{n \in s\}$ the set of towers belonging to overhead transmission line ω p_i the failure probability of transmission tower h $\{g \in \rho\}$ Parameters and constants p_i p_i the f	h [']	index of power transmission line segment	**,*	
$\begin{array}{cccccccccccccccccccccccccccccccccccc$	g	index of gas pipeline segment	C_n	the planning-oriented economic index of component <i>n</i>
$ \begin{array}{c} \frac{Q_s^k}{Q_s^k} & \text{the k-order subset of s} \\ TD & \text{the set of potential disaster scenarios} \\ D_l & \text{the set of potential disaster scenarios} \\ D_l & \text{the set of potential Type-l disaster scenarios} \\ RD & \text{the set of figs-j} under all potential disaster scenarios} \\ RD & \text{the set of failed components} \\ \{n \in s\} \\ \{h \in \omega\} \\ \text{the set of failed components} \\ \{h \in \omega\} \\ \text{the set of Inne segments belonging to overhead transmission line ω} \\ \{h \in \omega\} \\ \text{the set of line segments belonging to overhead} \\ \text{transmission line ω} \\ \{g \in \rho\} \\ \text{the set of pipeline segments belonging to overhead} \\ \text{transmission line ω} \\ \{g \in \rho\} \\ \text{the set of pipeline segments belonging to gas pipeline ρ} \\ Parameters and constants \\ q & \text{the low calorific value of natural gas} \\ N & \text{number of components in IEGS} \\ n_s & \text{the cardinality of TD} \\ K_l & \text{the cardinality of TD} \\ K_l & \text{the cardinality of TD} \\ K_l & \text{the cardinality of TD} \\ M_u & \text{upper limit of earthquake magnitude} \\ M_0 & \text{lower limit of earthquake magnitude} \\ N_s & \text{number of the enumerated points in the ith latent source} \\ region \\ a_l & \text{activity weight of the ith latent source region} \\ R_l & \text{the earthquake damage rate} \\ \end{array} \begin{array}{c} x, y & \text{horizontal and vertical coordinates of the epicentre distance} \\ P_r & \text{the probability of the arthquake magnitude} \\ N_s & \text{the failure probability of transmission line segment g} \\ N_p & \text{the failure probability of transmission line segment g} \\ N_0 & \text{the cardinality of TD} \\ N_0 & \text{the maximum wind speed at time t} \\ \text{the central pressure difference at time t} \\ \text{the maximum wind speed at time t} \\ \text{the maximum wind speed at time t} \\ \text$	S	fault state denoted by the set of failure components	H_n	the strengthening cost for component <i>n</i>
The set of potential disaster scenarios D_l the set of potential Type- l disaster scenarios D_l the set of potential Type- l disaster scenarios D_l the set of $r_{Sys,i}$ under all potential disaster scenarios p_r the probability of each basic disaster parameter p_r the set of fine outer boundary of intensity p_r the set of incomponents p_r the set of line segments belonging to overhead transmission line p_r the set of pipeline segments belonging to gas pipeline p_r the failure probability of transmission tower p_r the failure probability of pipeline segment p_r the failure probability of pipeline p_r the failure probabi	Ω_j	the set of <i>j</i> -order fault states	M	
$\begin{array}{llllllllllllllllllllllllllllllllllll$	Ω_s^k	the <i>k</i> -order subset of <i>s</i>		horizontal and vertical coordinates of the epicentre
RD the set of $r_{sys.i}$ under all potential disaster scenarios $\{n \in s\}$ the set of failed components $\{n \in s\}$ the set of non-failed components $\{n \in s\}$ the set of non-failed components $\{n \in s\}$ the set of lowers belonging to overhead transmission line ω the set of line segments belonging to overhead transmission line ω the set of line segments belonging to overhead transmission line ω the set of line segments belonging to gas pipeline ρ the set of pipeline segments belonging to gas pipeline ρ the set of pipeline segments belonging to gas pipeline ρ the failure probability of transmission line segment g the set of pipeline segments belonging to gas pipeline ρ the failure probability of pipeline segment g the failure probability of transformer τ the failure probability of overhead transmission the failure probability of sas pipeline ρ the failure probability of overhead transmission the failure probability of overhead transmission the failure probability of fast probability of overhead transmission the failure probability of transformer τ the failure probability of overhead transmission the failure probability of tran		•		•
$ \{n \notin s\} $ the set of non-failed components $ \{h \in \omega\} $ the set of towers belonging to overhead transmission line ω $ \{h \in \omega\} $ the set of line segments belonging to overhead transmission line ω $ \{g \in \rho\} $ the set of pipeline segments belonging to gas pipeline ρ $ Parameters \ and \ constants $ $ q $				
	,			•
$ \{h \in \omega\} \text{ the set of line segments belonging to overhead transmission line } \omega \\ \{g \in \rho\} \text{ the set of pipeline segments belonging to gas pipeline } \rho \\ Parameters and constants \\ q \text{ the low calorific value of natural gas } \\ N \text{ number of components in IEGS} \\ n_s \text{ the cardinality of } TD \\ K_l \text{ the annual frequency of Type-}l \text{ disaster } L \text{ number of disaster types considered } M_u \text{ upper limit of earthquake magnitude } M_0 \text{ lower limit of earthquake magnitude } M_0 \text{ span of the earthquake magnitude } M_0 \text{ number of the enumerated points in the ith latent source region } \alpha_l \text{ activity weight of the } ith latent source region } m_l \text{ the failure probability of transmission line segment } M_{\lambda g} \text{ the failure probability of transmission tower half all the failure probability of transmission of the failure probability of gas pipeline } \rho the failure probability of transmission tower half all the failure probability of transmission the failure probability of transmission the failure probability of transformer \tau the failure probability of transformer \tau the failure probability of transmission tower half all the failure probability of transmission the failure probability of transmission the failure probability of transmission the failure probability of gas pipeline \rho horizontal and vertical coordinates of the typhon site of the clockwise angle between typhon motion direction the coordinates of the typhon moving speed the coordinates of the typhon moving speed when the probability of transmission to the top original central pressure difference the typhon moving speed to time t the maximum wind speed at time t the maximum wind speed at time t the maximum wind speed at time t the typhon duration time (h) the real-time wind speed of tower h the failure probability of transmission tower h and the failure probabili$	1. ' 1.			
transmission line ω $\{g \in \rho\}$ the set of pipeline segments belonging to gas pipeline ρ Parameters and constants q the low calorific value of natural gas N number of components in IEGS n_s the cardinality of fault state s J the maximum enumeration fault order K the cardinality of TD K_l the cardinality of D_l L number of disaster types considered M_u upper limit of earthquake magnitude ΔM span of the earthquake magnitude ΔM span of the earthquake magnitude ΔM span of the enumerated points in the i th latent source region α_i activity weight of the i th latent source region α_i activity weight of the i th latent source region α_i activity weight of the i th latent source region α_i the failure probability of pipeline segment g the failure probability of pipeline segment g the failure probability of pipeline segment g the failure probability of pripeline segment g the failure probability of verhead transmission the failure probability of pripeline segment g the failure probability of verhead transmission the failure probability of pripeline segment g the failure probability of verhead transmission the failure probability of verhead transmission the failure probability of probability of verhead transmission the failure probability of verhead transmission the failure probability of verhead transmission the failure	,			
$ \begin{cases} g \in \rho \} & \text{the set of pipeline segments belonging to gas pipeline } \rho \\ Parameters and constants \\ q & \text{the low calorific value of natural gas} \\ N & \text{number of components in IEGS} \\ N_s & \text{the cardinality of fault state } s \\ J & \text{the maximum enumeration fault order} \\ K & \text{the cardinality of } TD \\ K_l & \text{the cardinality of } TD \\ K_l & \text{the annual frequency of Type-} l \text{ disaster} \\ L & \text{number of disaster types considered} \\ M_u & \text{upper limit of earthquake magnitude} \\ M_0 & \text{lower limit of earthquake magnitude} \\ M_N_s & \text{number of latent source regions in the seismic statistical area} \\ C_i & \text{number of the enumerated points in the } i\text{th latent source} \\ region \\ C_i & \text{activity weight of the } i\text{th latent source region} \\ C_i & \text{activity weight of the } i\text{th latent source region} \\ R_f & \text{the earthquake damage rate} \end{cases} $ The failure probability of transformer τ the failure probability of overhead transmission the failu	(12 C W)	0 0		
Parameters and constants q the low calorific value of natural gas N number of components in IEGS N_s the cardinality of fault state s N_s the maximum enumeration fault order N_s the cardinality of N_s	$\{g \in \rho\}$			
the low calorific value of natural gas N number of components in IEGS N_s the cardinality of fault state s N_s the cardinality of fault order N_s the cardinality of TD N_s the cardinality of TD N_s the cardinality of TD N_s the annual frequency of Type- t disaster N_s upper limit of earthquake magnitude N_s number of latent source region N_s number of the enumerated points in the t th latent source region N_s the cardinality of t the failure probability of gas pipeline t the typhod site N_s the cardinality of t the typhod morizontal and vertical coordinates of the typhod site N_s the cardinality of t the typhod motion direction N_s the cardinality of t the cardinality of t the original central pressure difference the typhod moving speed N_s the cordinality of t the original central pressure difference the typhod moving speed to the real-time wind speed at time t the central pressure difference at time t the central pressure difference at time t the maximum wind speed radius at time t the maximum wind speed at time t the maximum wind speed at time t distance from the typhoon centre at time t the typhod duration time (h) N_s number of the enumerated points in the t th latent source region N_s number of the enumerated points in the t th latent source region N_s number of the enumerated points in the t th latent source region N_s the failure probability of gas pipeline t the typhod moving speed time t the typhod duration time (h) N_s the failure probability of transmission tower t and the fai				
Nonumber of components in IEGS n_s the cardinality of fault state s J the maximum enumeration fault order K the cardinality of TD K_l the cardinality of D_l t the annual frequency of Type- l disaster t the annual frequency of Type- l disaster t the upper limit of earthquake magnitude t upper limit of earthquake magnitude t the contral pressure difference at time t the central pressure difference at time t the real-time wind speed at time t the maximum wind speed radius at time t the maximum wind speed at time t the typhoon centre at time t the typhoon duration time (h) t the real-time wind speed of tower t the typhoon duration time (h) t the real-time wind speed of line segment t the failure probability of transmission tower t and t the failure probability of transmission tower t and t the failure probability of transmission tower t and t the failure probability of transmission tower t and t the failure probability of transmission tower t and t the failure probability of transmission tower t and t the failure probability of transmission tower t and t the failure probability of transmission tower t and t the failure probability of transmission tower t and t the failure probability of transmission tower t and t the failure probability of transmission tower t and t the failure probability of transmission tower t and t the failure probability of transmission tower t and t the failure probability of transmission tower t and t the failure probability of transmission tower t and t the failure probability of transmission tower t and t the failure				
The cardinality of fault state s J the maximum enumeration fault order K the cardinality of TD K_l the cardinality of D_l ΔH_0 the original central pressure difference S_l the annual frequency of Type- S_l disaster S_l the property of the annual frequency of Type- S_l disaster S_l the annual frequency of Type- S_l disaster S_l the typhoon moving speed S_l the real-time wind speed at time S_l the maximum wind speed at time S_l distance from the typhoon centre at time S_l the typhoon duration time S_l the real-time wind speed of tower S_l the real-time wind speed of line segment S_l the failure probability of transmission tower S_l and S_l the failure probability of transmission tower S_l and S_l the failure probability of transmission tower S_l and S_l the failure probability of transmission tower S_l the				horizontal and vertical coordinates of the typhoon landing
the maximum enumeration fault order K the cardinality of TD K_l the cardinality of D_l the annual frequency of Type- l disaster L number of disaster types considered M_u upper limit of earthquake magnitude ΔM span of the earthquake magnitude ΔM span of the earthquake magnitude S_l number of latent source region S_l activity weight of the I the the typhoon moving speed I the real-time wind speed at time I the maximum wind speed at time I the maximum wind speed radius at time I the maximum wind speed at time I the typhoon duration time I the typhoon duration time I the typhoon duration time I the real-time wind speed of tower I the real-time wind speed of line segment I the failure probability of transmission tower I and I the failure probability of transmission tower I and I the failure probability of transmission tower I and I the failure probability of transmission tower I and I the failure probability of transmission tower I and I the failure probability of transmission tower I and I the failure probability of transmission tower I and I the failure probability of transmission tower I and I the failure probability of transmission tower I and I the failure probability of transmission tower I and I the failure probability of transmission tower I and I the failure probability of transmission tower I the failure probability of transmission		-		
$ \begin{array}{cccccccccccccccccccccccccccccccccccc$			θ	the clockwise angle between typhoon motion direction and
K_l the cardinality of D_l the annual frequency of Type- l disaster L number of disaster types considered M_u upper limit of earthquake magnitude M_0 lower limit of earthquake magnitude M_0 span of the earthquake magnitude M_0 span of the earthquake magnitude segment M_s number of latent source regions in the seismic statistical area C_i number of the enumerated points in the i th latent source region M_0 the real-time wind speed at time t the maximum wind speed radius at time t the maximum wind speed at time t distance from the typhoon centre at time t M_0 the real-time wind speed of tower M_0 the real-time wind speed of tower M_0 the real-time wind speed of line segment M_0 the failure probability of transmission tower M_0 activity weight of the M_0 the earthquake damage rate				
the annual frequency of Type- l disaster L number of disaster types considered L number of disaster types considered L number of disaster types considered L upper limit of earthquake magnitude L the central pressure difference at time L the maximum wind speed radius at time L the maximum wind speed radius at time L the maximum wind speed at time L distance from the typhoon centre at time L area L the typhoon duration time L the real-time wind speed of tower L the real-time wind speed of line segment L the failure probability of transmission tower L and L the failure probability of transmission tower L and L the failure probability of transmission tower L and L the failure probability of transmission tower L and L the failure probability of transmission tower L and L the failure probability of transmission tower L and L the failure probability of transmission tower L and L the failure probability of transmission tower L and L the failure probability of transmission tower L and L the failure probability of transmission tower L and L the failure probability of transmission tower L and L the failure probability of transmission tower L and L		•	ΔH_0	
L number of disaster types considered M_u upper limit of earthquake magnitude M_0 lower limit of earthquake magnitude ΔM span of the earthquake magnitude segment N_s number of latent source regions in the seismic statistical area c_i number of the enumerated points in the i th latent source region α_i activity weight of the i th latent source region α_i the earthquake damage rate c_i number of the enumerated points in the i th latent source region c_i activity weight of the i th latent source region c_i the failure probability of transmission tower h aduring typhoon c_i the failure probability of transmission tower h aduring typhoon c_i the failure probability of transmission tower h aduring typhoon				
M_u upper limit of earthquake magnitude M_0 lower limit of earthquake magnitude M_0 span of the earthquake magnitude segment N_s number of latent source regions in the seismic statistical area C_i number of the enumerated points in the i th latent source region C_i activity weight of the i th latent source region C_i the earthquake damage rate C_i the central pressure difference at time t the maximum wind speed at time t the maximum wind speed at time t the maximum wind speed at time t the typhoon duration time (h) C_i the real-time wind speed of tower t the real-time wind speed of line segment t the failure probability of transmission tower t and t the failure probability of transmission tower t and t the failure probability of transmission tower t and t the failure probability of transmission tower t and t the failure probability of transmission tower t and t the failure probability of transmission tower t and t the failure probability of transmission tower t and t the failure probability of transmission tower t and t the failure probability of transmission tower t and t the failure probability of transmission tower t and t the failure probability of transmission tower t and t the failure probability of transmission tower t and t the failure probability of transmission tower t and t the failure probability of transmission tower t and t the failure probability of transmission tower t and t the failure probability of transmission tower t and t the failure probability of transmission tower t and t the failure probability of transmission tower t and t the central pressure difference at time t the maximum wind speed at time t the ma				
ΔM span of the earthquake magnitude segment N_s number of latent source regions in the seismic statistical area c_i number of the enumerated points in the i th latent source region c_i activity weight of the i th latent source region c_i activity weight of the i th latent source region c_i activity weight of the i th latent source region c_i activity weight of the i th latent source region c_i the earthquake damage rate c_i the maximum wind speed at time t distance from the typhoon centre at time t the typhoon duration time (h) the real-time wind speed of tower t the failure probability of transmission tower t and t the failure probabil	M_u		` '	
N_s number of latent source regions in the seismic statistical area C_i number of the enumerated points in the i th latent source region C_i number of the enumerated points in the i th latent source region C_i activity weight of the i th latent source region C_i the earthquake damage rate C_i distance from the typhoon centre at time i th the typhoon duration time i th the typhoon duration time i th the real-time wind speed of tower i th the real-time wind speed of line segment i th the failure probability of transmission tower i th failure probability of transmission tower i t	M_0			=
T the typhoon duration time (h) c_i number of the enumerated points in the i th latent source region α_i activity weight of the i th latent source region R_f the earthquake damage rate T the typhoon duration time (h) $v_h(t)$ the real-time wind speed of tower h the real-time wind speed of line segment h the failure probability of transmission tower h a during typhoon				
number of the enumerated points in the <i>i</i> th latent source region $v_h(t)$ the real-time wind speed of tower h the real-time wind speed of line segment h the failure probability of transmission tower h activity weight of the <i>i</i> th latent source region R_f the earthquake damage rate $v_h(t)$ the failure probability of transmission tower h and h the failure probability of h the fail	N_s			
region $v_h(t)$ the real-time wind speed of line segment h the failure probability of transmission tower h a during typhoon R_f the earthquake damage rate				
α_i activity weight of the <i>i</i> th latent source region $\delta_h(t)$ the failure probability of transmission tower <i>h</i> a during typhoon $\delta_h(t)$ the failure probability of transmission tower <i>h</i> and $\delta_h(t)$ the failure probability of transmission tower <i>h</i> and $\delta_h(t)$ the failure probability of transmission tower <i>h</i> and $\delta_h(t)$ the failure probability of transmission tower <i>h</i> and $\delta_h(t)$ the failure probability of transmission tower <i>h</i> and $\delta_h(t)$ the failure probability of transmission tower <i>h</i> and $\delta_h(t)$ the failure probability of transmission tower <i>h</i> and $\delta_h(t)$ the failure probability of transmission tower <i>h</i> and $\delta_h(t)$ the failure probability of transmission tower <i>h</i> and $\delta_h(t)$ the failure probability of transmission tower <i>h</i> and $\delta_h(t)$ the failure probability of transmission tower <i>h</i> and $\delta_h(t)$ the failure probability of transmission tower <i>h</i> and $\delta_h(t)$ the failure probability of transmission tower <i>h</i> and $\delta_h(t)$ the failure probability of transmission tower <i>h</i> and $\delta_h(t)$ the failure probability of transmission tower <i>h</i> and $\delta_h(t)$ the failure probability of transmission tower <i>h</i> and $\delta_h(t)$ the failure probability of transmission tower <i>h</i> and $\delta_h(t)$ the failure probability of transmission tower <i>h</i> and $\delta_h(t)$ the failure probability of transmission tower <i>h</i> and $\delta_h(t)$ the failure probability of transmission tower <i>h</i> and $\delta_h(t)$ the failure probability of transmission tower <i>h</i> and $\delta_h(t)$ the failure probability of transmission tower <i>h</i> and $\delta_h(t)$ the failure probability of transmission tower <i>h</i> and $\delta_h(t)$ the failure probability of transmission tower <i>h</i> and $\delta_h(t)$ the failure probability of transmission tower <i>h</i> and $\delta_h(t)$ the failure probability of transmission tower <i>h</i> and $\delta_h(t)$ the failure probability of transmission tower <i>h</i> and $\delta_h(t)$ the failure probability of transmission tower <i>h</i> and $\delta_h(t)$ the failure probability of transmission tower <i>h</i> and $\delta_h(t)$ the failure probability of transmission tower <i>h</i> and $\delta_h(t)$ the failure pr	c_i	-		
R_f the earthquake damage rate during typhoon	a:	=		the failure probability of transmission tower h at time t
(c) the Callinguage rate			,	
Δy ichigh of pipeline segment $\frac{\partial u(y)}{\partial y}$ the fainte probability of datasmosion line segment	Δg	length of pipeline segment	$\delta_h(t)$	the failure probability of transmission line segment h' at
S length of the coastline time t during typhoon	_			
ds the segment intervals of S				

oriented resilience index [11] only considers the robustness and is defined as the weighted average of the load shedding expectations under all potential typhoon scenarios. This simplification is feasible for the transmission system, which mainly focuses on the ability to withstand disasters

IEGS is an important form of the *trans*-regional integrated energy system, which connects electrical power system (EPS) and natural gas system (NGS) through coupling facilities. In recent years, research on the resilience of IEGS has been paid increasing attention. Ref. [12] draws the intensity distribution map according to the earthquake intensity attenuation characteristic to assess the resilience of IEGS crossing different intensity regions. Ref. [11] builds a cumulative component failure probability model to describe the typhoon impact. Ref. [13] uses the buried gas pipelines to improve the EPS resilience from the perspective of the coordinated planning of EPS and NGS. In reality, IEGS is subject to various types of disasters, while existing studies usually perform resilience assessment in terms of single-type disaster. A resilient IEGS should be planned with sufficient resilience under any possible disaster, which places a demand on resilience assessment considering multi-type disasters.

The methods for resilience assessment can be divided into Monte Carlo Simulation (MCS) -based and analytical methods, such as state enumeration (SE). The fault states of MCS are sampled according to the component failure probability, which is changed under different disaster scenarios. SE generally enumerates only low-order fault states to ensure efficiency, leading to a certain underestimation. As an improvement of SE, the impact-increment-based state enumeration (IISE) method increases the weight of low-order fault states, thereby significantly reducing the error caused by ignoring high-order fault states [14,36]. In addition, the impact-increments obtained by IISE can be reused when the disaster scenario changes, which is a huge advantage over MCS.

Existing research on resilience enhancement mainly includes Robust Optimization (RO) -based and scenarios-based methods [15]. The RO-based method generally builds a tri-level defender-attacker-defender model to optimize the resilience performance in the worst case [16,17], leading to a pessimistic resilience enhancement scheme. The scenarios-based method analyses the impact of each disaster scenario generated according to historical data [11,18], thus finding the system weaknesses for targeted reinforcement. However, this method is quite time-consuming.

To sum up, the diversity of natural disaster types is rarely considered in previous resilience studies and may lead to one-sided results. This concern is even more pronounced in some areas with more than one type of major disasters, such as Indonesia and Taiwan [19,20]. When it comes to the index calculation, MCS has to resample fault states considering multi-type disasters, while the accuracy of SE is often not up to requirement. To this end, this paper proposes a resilience assessment and enhancement approach for IEGS planning considering multi-type natural disasters. The main contributions are as follows:

- 1) A unified natural disaster modelling framework has been developed to extract the key information of potential disasters as one intuitive format, which allows us to generate the disaster scenario database covering multi-type disasters for planning investigations.
- 2) The IISE method has been extended to develop a resilience assessment method considering a large number of potential disaster scenarios. This is achieved by repeatedly invoking the impact-increment database during the assessment and leads to significant computational efficiency improvement.
- 3) Both the component-level resilience indices and economic indices are proposed to help planners identify the most suitable resilience enhancement scheme.

2. Basic theory

2.1. Resilience indices

As for planning of IEGS, robustness generally has a higher weighting than other resilience factors. To simplify the calculation, a system-level resilience index $r_{\rm sys}$ is denoted to quantify the resilience of the IEGS, which is expressed as

$$r_{svs} = E[Q_{shed}] \tag{1}$$

$$Q_{shed} = P_{shed} + qG_{shed} \tag{2}$$

where $E[Q_{shed}]$ is the expected load shedding (MW); P_{shed} and G_{shed} are the shedding of electric load (MW) and natural gas load (Sm³/h) respectively; q is the low calorific value of natural gas, taken as 0.01045MWh/Sm³. The smaller the r_{sys} , the stronger the resilience of IEGS

The component-level index r_n' proposed in Ref. [21] describes the contribution of each component to the system-level resilience index. This index can help accurately locate the weak points of IEGS, so as to make effective resilience enhancement strategies. However, the original index r_n' is not well suited to the formulation of resilience enhancement scheme, which is explained in Appendix A. In this paper, r_n' is modified to r_n by

$$r'_{n} = r_{sys} - r_{sys}|_{p_{n}=0} \rightarrow r_{n} = r_{sys} - r_{sys}|_{p_{n}=p'_{n}}$$
 (3)

where $r_{\rm sys}|_{p_n=0}$ and $r_{\rm sys}|_{p_n=p'_n}$ are the system-level resilience index after the failure probability of component n is reduced to 0 and p'_n respectively; p'_n is the failure probability of component n after strengthening. It can be seen from Eq. (3) that the component-level index is redefined as the effect of the strengthening measure for component n in this paper.

2.2. IISE method

The centrepiece of obtaining the resilience indices is the calculation of the expected load shedding, $E[Q_{shed}]$. According to the SE method, $E[Q_{shed}]$ is obtained by [14]

$$E[Q_{shed}] = \sum_{j=1}^{N} \sum_{s \in \Omega_j} \left[\left(\prod_{n \in s} p_n \right) \prod_{n \notin s} (1 - p_n) \right] I_s$$
 (4)

IISE method transforms Eq. (4) into Eq. (5)-(6).

$$E[Q_{shed}] = \sum_{i=1}^{N} \sum_{s \in \Omega_i} \left(\prod_{n \in s} p_n \right) \Delta I_s \tag{5}$$

$$\Delta I_s = I_s + \sum_{k=1}^{n_s - 1} (-1)^{n_s - k} \sum_{u \in O^k} I_u$$
 (6)

In Eq. (5), the successive multiplication of component failure probabilities can be regarded as the weight of impact-increment, which is falling rapidly as the failure order j increases. In addition, high-order impact-increment is close to 0, because the impact of fault states in IEGS have a certain degree of additivity. Therefore, the proportion of high-order parts in Eq. (5) is much smaller than that in Eq. (4).

Usually, only the low-order faults are enumerated to ensure computational efficiency. In this case, Eq. (5) is rewritten as Eq. (7) by introducing a maximum enumeration fault order, J. For IISE method, the error caused by ignoring the high-order faults shall be much smaller than SE method.

$$E[Q_{shed}] = \sum_{i=1}^{J} \sum_{s \in \mathcal{Q}_i} (\prod_{n \in s} p_n) \Delta I_s$$
 (7)

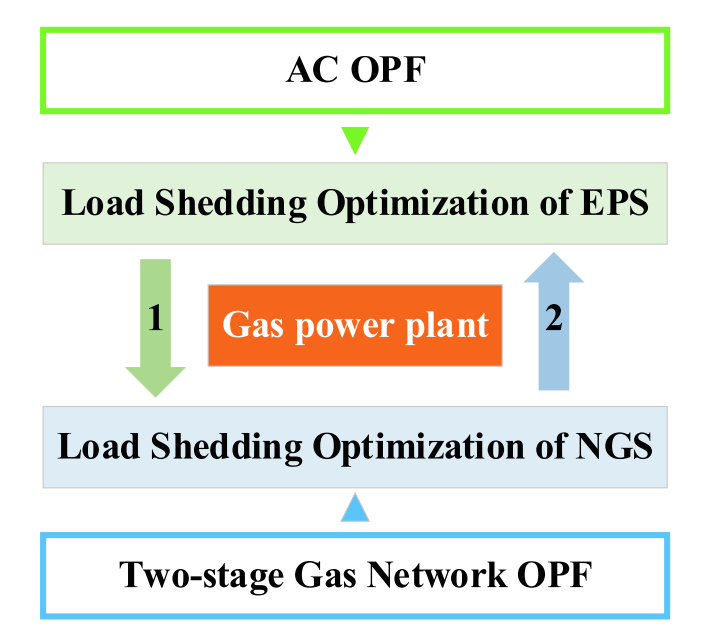


Fig. 1. The optimal load shedding algorithm for IEGS.

2.3. Optimal load shedding algorithm for IEGS

To reflect the role of emergency dispatch under faults, an efficient optimization algorithm is required to calculate the optimal load shedding of IEGS, which is the basis of IISE method. See Fig. 1

The decoupled framework is used in the optimal load shedding algorithm to improve computational efficiency. As Fig. 8 shows, the load shedding optimization of EPS and NGS are carried out separately. This paper connects EPS and NGS through gas power plant, which has been widely used in IEGS [17]. Denote the NGS node connected to gas power plant as GPP node. Then, arrow 1 indicates that the gas supply load in GPP node is determined based on the output of gas power plant from the EPS optimization result, while arrow 2 indicates that the output upper limit of gas power plant is reduced according to the gas load shedding of GPP node from the NGS optimization result. The EPS optimization module and the NGS optimization module iterate alternately until the gas supply load required by the gas power plants is no longer cut down in NGS.

Another advantage of decoupled optimization framework is that the large number of complex constraints of IEGS are split into two parts, allowing more accurate models to be applied to the subsystems. EPS optimization module is based on AC optimal power flow (OPF) model, which can be calculated using Matpower toolbox. NGS optimization module is based on two-stage gas network OPF model [22], which

integrated the mixed integer linear simplified model of stage 1 and the nonlinear continuous model of stage 2. As Fig. 2 shows, stage 1 obtains the approximate solutions of real and integer variables respectively. The former provides initial values for the interior point method in stage 2, while the later serves as the fixed input value of stage 2. In other words, stage 2 reasonably corrects the approximate solutions of stage 1. It is worth mentioning that the models in stage 1 and stage 2 can be handled by Cplex and Ipopt, both of which are mature solvers.

Although the decoupled optimization framework is not able to optimize electric load shedding and gas load shedding at the same time, the calculation results still own good application value. This is because EPS and NGS are usually operated by different utilities [17], while decoupled optimization framework is a good fit of the reality.

3. Planning-oriented resilience assessment and enhancement considering Multi-type natural disasters

There is serious uncertainty about the natural disasters to which IEGS may be exposed during the planning period. However, the resilience indices introduced in section 2.1 are only applicable to IEGS under a specific natural disaster. Due to this concern, this paper argues that planning-oriented resilience assessment should be based on a set of scenarios covering multi-type disasters, thus supporting objective decision-making.

The weighting method can be used to synthesize the resilience indices under each potential disaster scenario. However, two questions remain to be solved:

Q1: models for different types of natural disasters are considerably different, and there is lack of a unified framework for resilience assessment.

Q2: the number of potential disaster scenarios is huge, which makes it time-consuming to calculate the impact of all scenarios.

In this chapter, the proposed resilience assessment and enhancement method considering multi-type disasters is shown, including 1) the planning-oriented resilience indices considering the uncertainty of potential natural disasters; 2) generation of disaster scenario database to solve Q1 by integrating various potential disasters into the same format; 3) development of the impact-increment database to solve Q2 by storing the reusable parts of IISE method and 4) resilient planning using the two databases.

3.1. Planning-oriented resilience indices

The set of disaster scenarios that may occur in the study area is noted as TD, while the ith potential disaster scenario in TD is noted as d_i . According to the characteristic information of each potential disaster scenario, the resilience indices $r_{sys,i}$, $r_{n,i}$ under scenario d_i can be calculated by Eq. (1)-(3). In addition, the weight of the impact caused by scenario d_i

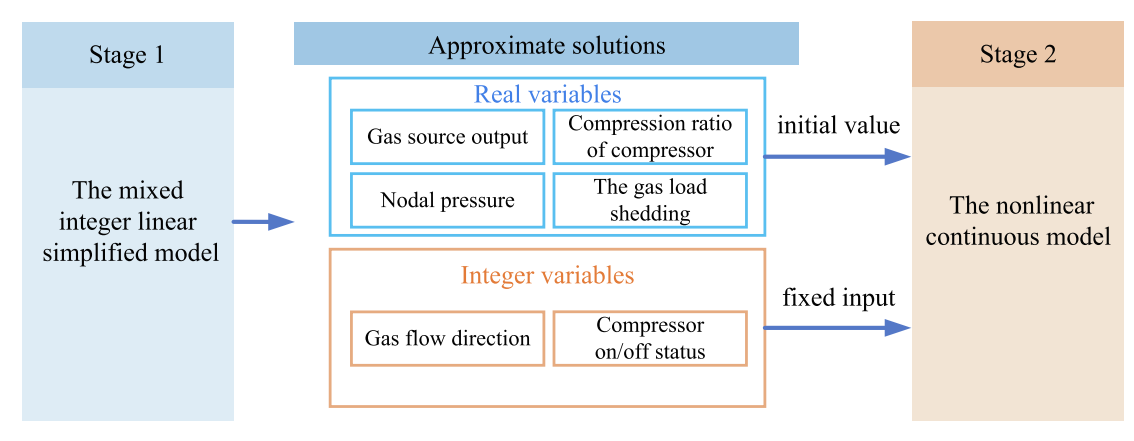


Fig. 2. Two-stage gas network optimal power flow model.

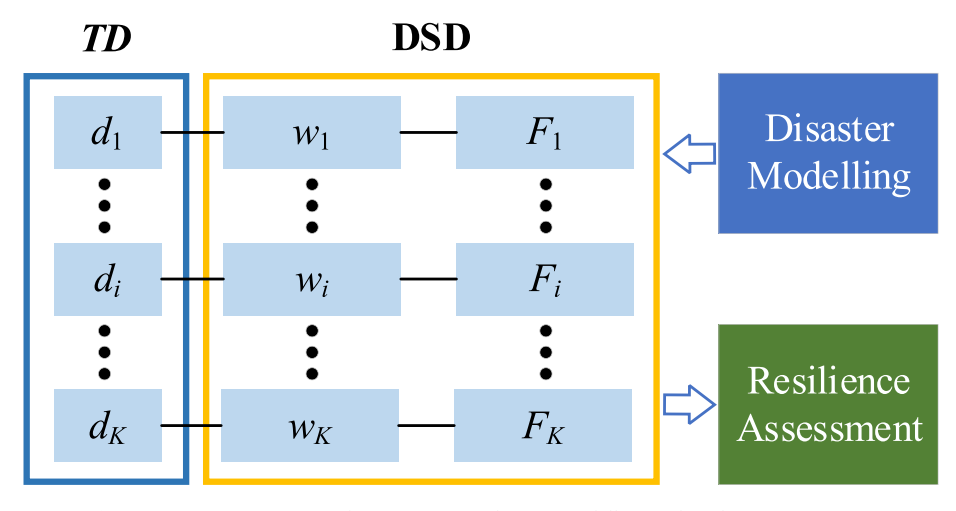


Fig. 3. Disaster Scenario Database connecting disaster modelling and resilience assessment.

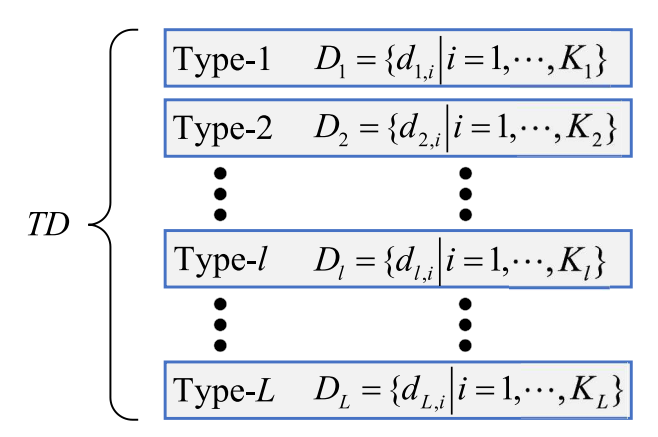


Fig. 4. The potential disaster scenario set covering multi-type disasters.

is noted as w_i , which is introduced in detail later.

The planning-oriented system-level resilience index R_{sys} is the weighted sum of r_{sys} , which is expressed as

$$R_{\text{sys}} = \sum_{i=1}^{K} w_i r_{\text{sys},i} \tag{8}$$

where K is the number of potential disaster scenarios in TD. The physical meaning of R_{sys} is the expected load shedding of IEGS after one natural disaster occurs.

Similarly, the planning-oriented component-level resilience index R_n is the weighted sum of r_n , which is expressed as

$$R_n = \sum_{i=1}^K w_i r_{n,i} \tag{9}$$

The economic index C_n is proposed to describe the cost-efficiency ratio of strengthening n, which is expressed as

$$C_n = \frac{H_n}{R_n} \tag{10}$$

where H_n represents the strengthening cost for component n.

When compared to r_{sys} and r_n , the planning-oriented indices are more comprehensive and reasonable as they take all potential disasters into consideration. In addition, R_n and C_n can assist planners in developing resilience enhancement schemes in terms of effectiveness and economy respectively.

3.2. Disaster scenario database

As Fig. 3 shows, each potential disaster scenario in TD is abstractly represented by the weight w_i and the component failure probability group F_i in the disaster scenario database (DSD), thus providing intuitive data support for the planning-oriented resilience assessment. In other words, DSD acts as an information bridge connecting disaster modelling and resilience assessment.

Considering the diversity of natural disaster types, all major disaster types in the study area are included in TD as shown in Fig. 4, where Type-l represents the disaster type l, such as earthquake, typhoon, etc., D_l is the set of potential Type-l disaster scenarios, K_l is the number of potential Type-l disaster scenarios, $d_{l,i}$ represents the ith scenario in D_l . The following relationship clearly exists:

$$\begin{cases}
TD = \bigcup_{l=1}^{L} D_l \\
K = \sum_{l=1}^{L} K_l
\end{cases}$$
(11)

The weight of disaster scenario $d_{l,i}$ is expressed as:

$$w_{l,i} = P_{l,i}f_l / \sum_{k=1}^{L} f_k \tag{12}$$

where $P_{l,i}$ is the conditional probability that the disaster scenario is d_l , under the premise that one Type-l disaster occurs, denoted as the occurrence probability of $d_{l,i}$ in a narrow sense, f_l is the annual frequency of Type-l disaster.

The component failure probability group of disaster scenario $d_{l,i}$ is expressed as:

$$F_{l,i} = \{ p_{li,1}, p_{li,2}, \dots, p_{li,n}, \dots, p_{li,N} \}$$
(13)

where $p_{li,n}$ is the failure probability of component n under disaster scenario d_{li} .

In order to construct DSD for resilience assessment, the modelling process of each natural disaster type considered needs to generate the potential disaster scenario subset D_l , as well as calculate the scenario weight $w_{l,i}$ and the component failure probability group $F_{l,i}$.

3.2.1. Unified research framework of natural disasters regardless of type

For any type of natural disaster, there shall be two categories of parameters: 1) basic parameter that determines a specific disaster scenario; 2) direct parameter that determines the failure probabilities of disaster-affected components. The former is the smallest parameter group that can describe a disaster, while the latter refers to disaster impact parameter that is directly related to the failure probability of

Fig. 5. The disaster scenario generation based on combinatorial enumeration method.

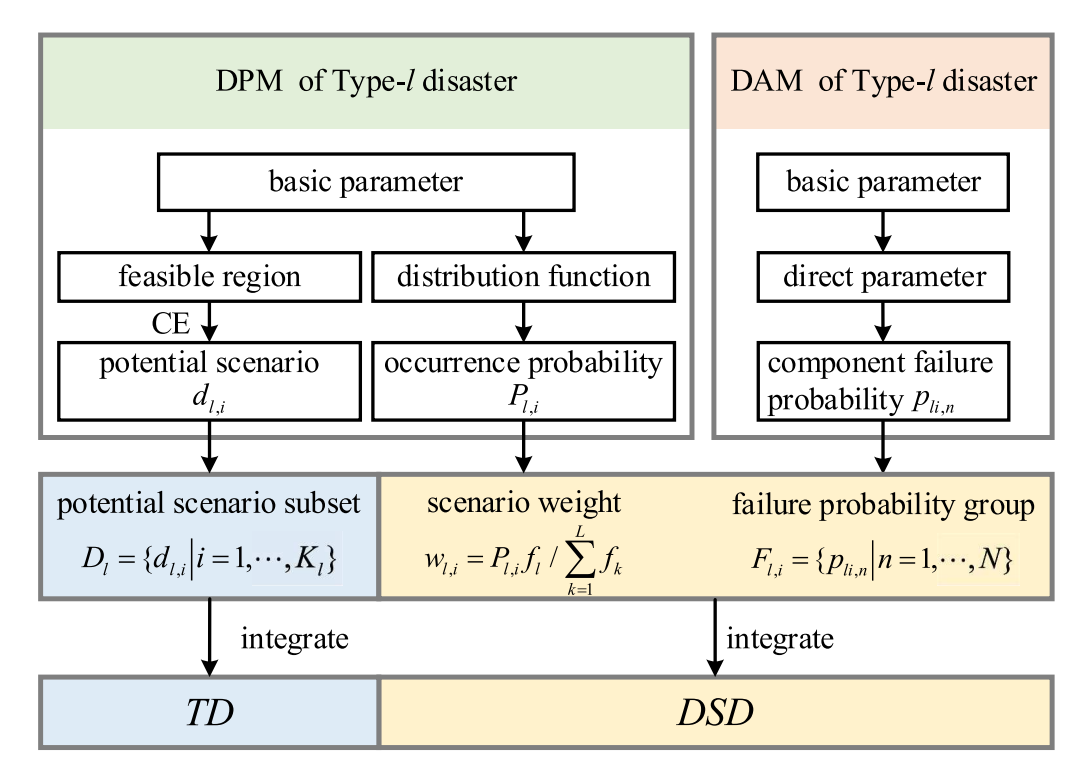


Fig. 6. The research framework of natural disaster modelling.

IEGS components. Disasters usually hit the study area unevenly, so the direct parameters of the components at various locations are generally different.

For example, the basic parameters of typhoon are the landing site, the motion direction, the original pressure difference, and the translational speed, while the direct parameter of typhoon-affected components is the real-time wind speed; the basic parameters of earthquake are the magnitude and the epicentre site, while the direct parameter of earthquake-affected components is the earthquake intensity.

The generation of potential disaster scenario is essentially the generation of basic parameter group. As shown in Fig. 5, the feasible region of each disaster basic parameter is equally divided into several intervals, which are enumerated and combined to generate disaster scenarios. For example, suppose that there are two basic parameters for a certain type of disaster, and that their feasible regions are divided into α parts and β parts respectively. Through the combinatorial enumeration (CE) method, a total of $\alpha\beta$ potential disaster scenarios can be generated. For ease of analysis, the midpoint of each interval is selected as the representative value.

In view of the need to construct DSD, this paper models natural

disaster from two perspectives. Disaster probability model (DPM) is established to describe the uncertainty of disaster scenarios, while disaster attack model (DAM) is established to describe the attack mode of each disaster scenario. As shown in Fig. 6, the DPM of Type-l disaster applies CE method to get the potential scenario subset $D_l = \{d_{l,i} | i=1,\cdots,K_l\}$ according to the feasible region of each basic parameter. In addition, DPM calculates the occurrence probability $P_{l,i}$ of each generated scenario $d_{l,i}$ based on basic parameter distribution functions, and then the scenario weight $w_{l,i}$ can be obtained by Eq. (12). The DAM of Type-l disaster should include the derivation process from the basic disaster parameter to the direct disaster parameter, which can be used to get the component failure probability group $F_{l,i}$ under each scenario $d_{l,i}$. The potential scenario subset D_l of each major disaster type is integrated into TD, while the $w_{l,i}$ and $F_{l,i}$ of each generated scenario are integrated into DSD.

3.2.2. The typical natural disaster modelling

Natural disasters mainly include extreme weather-driven disasters and geological disasters. The former is generally difficult to damage the buried components of NGS, while the latter can impact EPS and NGS at

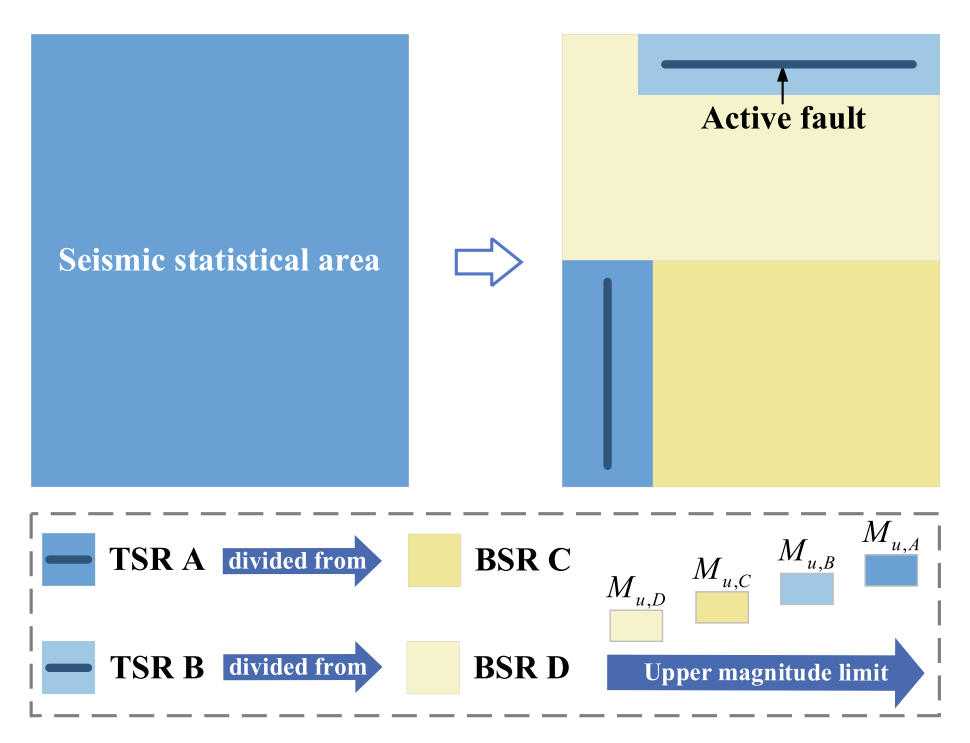


Fig. 7. Three-level delineation for latent earthquake sources.

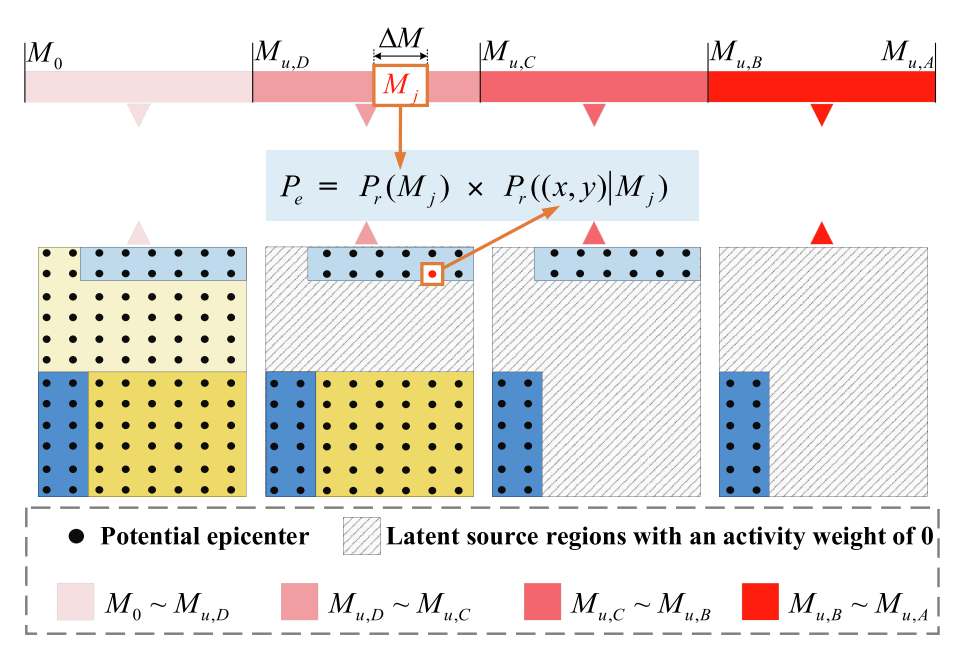


Fig. 8. The occurrence probability of the generated earthquake scenario.

the same time. In recent years, resilience research mainly focuses on weather-driven disasters. Therefore, this paper takes the most typical geological disaster, i.e., earthquake, as an example to introduce the proposed disaster modelling research framework in detail.

(1) Disaster Probability Model

To apply the CE method to earthquake disaster, it is necessary to determine the feasible region of earthquake magnitude M and epicentre site (x,y). According to the principle of three-level delineation for latent earthquake sources [23], the background source regions (BSR) are divided from the seismic statistical area, while the tectonic source regions (TSR) along active faults are divided from the background source region. As Fig. 7 shows, The upper magnitude limit of TSR is higher than

that of BSR to which it belongs $(M_{u,A} > M_{u,C}, M_{u,B} > M_{u,D})$, and the upper magnitude limit $M_{u,s}$ of seismic statistical area is the maximum upper magnitude limit of all tectonic source regions it contains $(M_{u,s} = \max [M_{u,A}, M_{u,B}, M_{u,C}, M_{u,D}])$. In addition, threshold magnitude M_0 describes the smallest earthquake magnitude that may influence IEGS, usually taken as 4.0. In this way, the feasible region of earthquake magnitude is $[M_0, M_{u,s}]$, which can be discretized into the magnitude segments; the feasible region of epicentre site is the entire seismic statistical area, which can be divided by the grid method.

According to Ref. [23], the distribution function of earth quake magnitude \boldsymbol{M} is expressed as

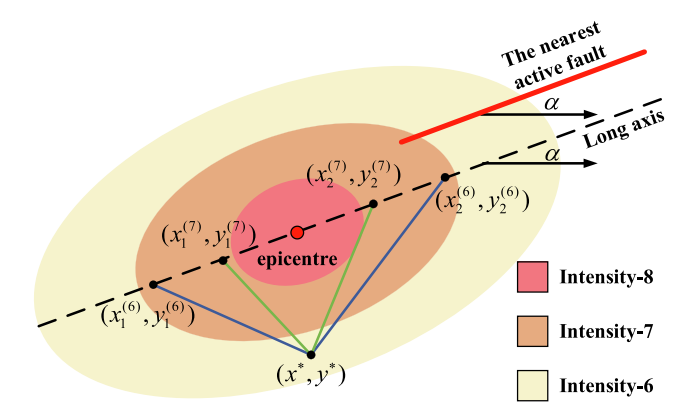


Fig. 9. Earthquake intensity distribution map.

$$P_r(M_j) = \frac{2exp[-bln10(M_j - M_0)]}{1 - exp[-bln10(M_{us} - M_0)]} \cdot sh(\frac{b}{2}\Delta Mln10)$$
 (14)

where M_j is the midpoint of the jth magnitude segment; ΔM is the span of the magnitude segment; b is the coefficient of the G-R relation, which represents the linear scale factor of the lg of earthquake frequency varying with magnitude [24].

The distribution of epicentre site is related to the earthquake magnitude, as earthquakes exceeding the M_u of a latent source region are considered to not occur in that region. After enumerating the potential epicentres by grid method, the probability that an earthquake belonging to the jth magnitude segment erupts at the enumerated point (x, y) within the ith latent source region can be obtained by [12]

$$P_r((x,y)|M_j) = \alpha_i/c_i \sum_{k=1}^{N_s} \alpha_k$$
(15)

where N_s is the number of latent source regions in the seismic statistical area; c_i is the number of the enumerated points in the ith latent source region; α_i is the activity weight of the ith latent source region, which is expressed as

$$\alpha_{i} = \begin{cases} c_{i} \times (M_{u,i} - M_{0}), & M_{j} \leq M_{u,i} \\ 0, & M_{j} > M_{u,i} \end{cases}$$
(16)

According to the upper magnitude limit of each latent source area, the feasible region $[M_0,M_{u,s}]$ is divided into several intervals, while each interval contains several magnitude segments. The set of potential epicentre points related to each magnitude interval is different, as there may be some latent source regions with an activity weight of 0.

As Fig. 8 shows, the magnitude segment is enumerated first, and then the potential epicentre points related to the magnitude interval to which the magnitude segment belongs. In this way, DPM obtains the potential earthquake scenario set $D_e = \{d_e\}$, which is incorporated into TD. Besides, the occurrence probability of earthquake scenario d_e is expressed as

$$P_e = P_r(M_j)P_r((x,y)|M_j)$$
(17)

(2) Disaster Attack Model

Existing studies describe earthquake damage in different ways. Ref. [25] considers the earthquake influence through the Cross-Impact Analysis of multi-stage events, which is difficult to be applied in the calculation of resilience indices as a qualitative method. Ref. [26,27] chose Peak Ground Acceleration (PGA), Peak Ground Velocity (PGV) and Peak Ground Displacement (PGD) to characterise the earthquake influence. In fact, the ground motion parameter PGA/PGV/PGD is proposed to quantify the physical meaning of earthquake intensity, and there is a corresponding relationship between them [28]. For the convenience of analysis, this paper selects earthquake intensity I as the direct earthquake parameter.

Unlike magnitude, which focuses on the strength of earthquake itself, intensity describes the extent of damage caused by the earthquake. The Chinese earthquake intensity scale is taken as intensity standard, and only the 6, 7, 8 degrees of intensity with research value are considered in this paper. As the seismic wave spreads around, the intensity *I* meets the elliptical attenuation model, which considers *iso*-intensity lines as several ellipses with the same centre and direction. Along the direction of long axis or short axis, the earthquake intensity is expressed as

Along the long axis:
$$I = A_1 + B_1 M + C_1 lg(\phi + \phi_1) \leftrightarrow \phi = 10^{\frac{I-A_1-B_1M}{C_1}} - \phi_1$$

Along the short axis: $I = A_2 + B_2 M + C_2 lg(\phi + \phi_2) \leftrightarrow \phi = 10^{\frac{I-A_2-B_2M}{C_2}} - \phi_2$
(18)

where A_1/A_2 , B_1/B_2 , C_1/C_2 and ϕ_1/ϕ_2 are the regression parameters; ϕ is the epicentre distance, which can be deduced inversely when I is known.

The elliptical centre of the *iso*-intensity line is the epicentre site (x, y), while the direction of the long axis is consistent with the active fault closest to the epicentre. To simplify the analysis, the area enclosed by the *iso*-intensity lines with intensity $(I \pm 0.5)$ is noted as intensity-I zone, where the intensity at any point is assumed as I. If the intensity at point (x_d, y_d) is equal to I_d , it needs to satisfy

$$\left\| \left(x_d - x_1^{(I_d)}, y_d - y_1^{(I_d)} \right) \right\| + \left\| \left(x_d - x_2^{(I_d)}, y_d - y_2^{(I_d)} \right) \right\| \le 2r_a^{(I_d)}$$

$$\left\| \left(x_d - x_1^{(I_{d+1})}, y_d - y_1^{(I_{d+1})} \right) \right\| + \left\| \left(x_d - x_2^{(I_{d+1})}, y_d - y_2^{(I_{d+1})} \right) \right\| > 2r_a^{(I_{d+1})}$$

$$(19)$$

where $||\cdot||$ is the Euclidean norm; $(x_1^{(I)}, y_1^{(I)})$ and $(x_2^{(I)}, y_2^{(I)})$ are the focal points of the outer boundary of intensity-I zone; $r_a^{(I)}$ is the long axis radius of the outer boundary of intensity-I zone.

As Fig. 9 shows, the intensity distribution map is composed of a series of multi-level-nested ellipses. Using Eq. (19) as a criterion, the intensity at point (x^*, y^*) can be determined to be 6° . In this way, the mapping from the basic parameters (earthquake magnitude and epicentre site) of a specific earthquake to the direct parameter (earthquake intensity) of each point in the study area is achieved.

Under the earthquake disaster, transformers and overhead lines in EPS and gas pipelines in NGS are at risk of damage. Therefore, it's necessary to construct the failure probability models of these components based on the direct parameter, *I*.

The failure probability p_{τ} of the transformer τ under different earthquake intensity can be directly obtained from the historical data statistics.

The overhead line is composed of towers and line segments connecting these towers, while the latter can decouple earthquake energy by low-frequency vibrations. Regard the overhead line under earthquake disaster as a series system of towers, then the failure probability of overhead line ω can be expressed as

$$p_{\omega} = 1 - \prod_{h=1}^{\infty} (1 - \lambda_h) \tag{20}$$

where $h \in \omega$ denotes the towers belonging to ω ; λ_h is the failure probability of tower h, which is related to the earthquake intensity.

The gas pipeline is divided into several pipeline segments, and the position of each segment is taken as its midpoint. In this way, the failure probability of gas pipeline ρ is expressed as

$$p_{\rho} = 1 - \prod_{\alpha \in \rho} (1 - \lambda_{\alpha'})$$
 (21)

where $g \in \rho$ denotes the pipeline segments belonging to ρ ; λ_g is the failure probability of pipeline segment g, which is obtained by

$$\lambda_{g} = 1 - e^{-R_{f}\Delta g} \tag{22}$$

where R_f is the earthquake damage rate, which is related to the natural gas pipeline material and geometry parameters; Δg is the length of the pipeline segment (km).

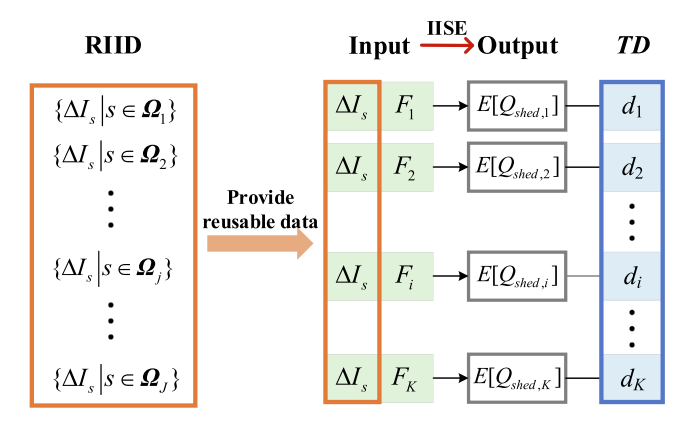


Fig. 10. Impact-Increment Database repeatedly invoked under each potential disaster scenario.

The spread of earthquake energy is so rapidly that the duration can be ignored in earthquake disaster model, while for some long-lasting weather-driven disasters, the overall impact during the disaster can be analysed according to the cumulative failure probability of components. As an example, typhoon modelling is introduced in detail in Appendix B. In addition, a list of other potential disaster types is given in Appendix B to illustrate the feasibility of including these disasters into DSD. It's worth noting that considering the safety of maintenance personnel, IEGS should not be repaired during a disaster.

3.3. Reusable Impact-Increment database

MCS method can improve and control the calculation accuracy by increasing the sampling times, which is the reason why its application popularity is much higher than that of SE method. When the disaster scenario changes, however, a new component failure probability group will force MCS to resample fault states, while the sampled fault states before cannot be used as reference. Worse still, the more disaster scenarios are considered, the more this shortcoming of MCS method will be magnified. Since *TD* contains quite a few potential disaster scenarios, the planning-oriented resilience assessment based on MCS method, while theoretically feasible, would be computationally costly in practice.

As an improved method of SE, IISE enhances the calculation accuracy to the level close to that of MCS. More importantly, the impact-increments obtained during the IISE calculation process, which are independent of the component failure probability, can be applied to any disaster scenario. This is the biggest advantage of IISE over MCS: it has

reusable parts.

As shown in Fig. 10, the impact-increments for fault states of order 1 to J are calculated in advance and stored into the database, which provides input to IISE method for solving the expected load shedding under each potential disaster scenario. Planning-oriented resilience assessment needs to solve the expected load shedding of IEGS under each potential disaster scenario one by one, while the calculation efficiency can be greatly improved by invoke the Reusable Impact-Increment Database (RIID). This is because, after removing the calculation of impact-increments, the calculation process of IISE method only leaves the basic addition and multiplication operations.

3.4. Resilient planning framework considering Multi-Type natural disasters

As Fig. 11 shows, the resilience indices under each potential disaster scenario are calculated efficiently according to the component failure probability F_i provided by DSD and the impact-increments ΔI provided by RIID. Then, the planning-oriented indices are solved by weighting and summing the obtained $r_{sys,i}$ and $r_{m,b}$, while the scenario weight w_i is provided by DSD. Resilient planning considering multi-type natural disasters includes the following steps:

Step 1: determine the main natural disaster types in the study area, as well as the basic and direct parameters of each type.

Step 2: apply the proposed disaster modelling research framework to each type of disaster, so as to build the DSD database covering multitype disasters.

Step 3: Calculate the impact-increments for IEGS fault states of order 1 to *J*, which are then stored in RIID database.

Step 4: Solve resilience indices r_{sys} and r_m using Eq.(1), (3) and (7), where the component failure probabilities and impact-increments are called from DSD and RIID respectively.

Step 5: Solve the planning-oriented resilience indices R_{sys} , R_m and C_m using Eq. (8), (9) and (10), where the weight of each potential scenario is called from DSD.

Step 6: R_{sys} is used to assess the system resilience considering the impact of all potential disaster scenarios, while R_m and C_m are used to determine the most suitable resilience enhancement scheme.

Case studies

3.5. Descriptions of test system

The test system is composed of the IEEE RTS 79 EPS and the 14-node NGS. As shown in Fig. 12, it includes 4 gas power plants, 33 overhead lines, 5 transformers, and 12 gas pipelines, with detailed data introduced

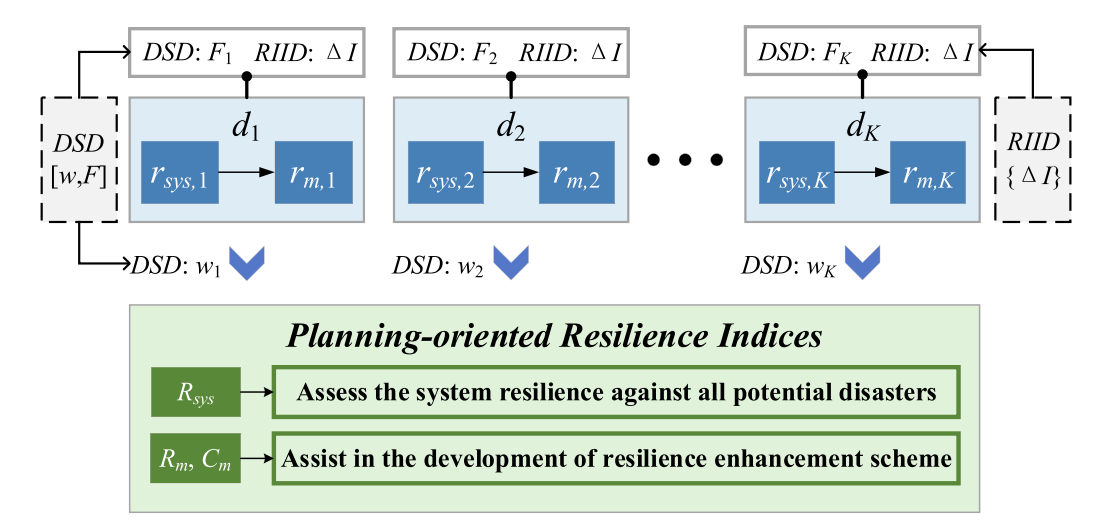


Fig. 11. Resilient planning framework based on DSD and RIID.

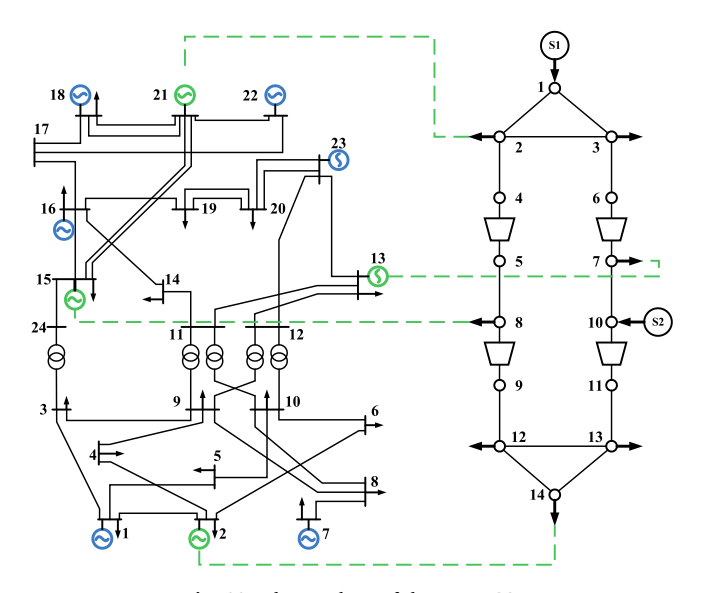


Fig. 12. The topology of the test IEGS.

in Appendix C.

The test IEGS is assumed to be in Taiwan, where typhoon and earthquake are the dominant natural disaster types. According to the Taiwan Central Weather Bureau, over the past decade, the annual average frequency of typhoons, f_w is 2.3, while that of earthquakes with

magnitude 4 or higher, f_e is 154.2. The rest of the disaster modelling parameters are given in Appendix D.

Fig. 13 depicts the spatial location of the test system attached to the simplified coastal seismic statistical zone, where EPS and NGS overlap each other that they need to be shown separately. The coastline is a straight line from (0, 0) to (250, 0), while the seismic statistical zone is divided into TSR A, TSR B, BSR C and BSR D, with the upper magnitude limits of 8.0, 7.5, 6.0, and 5.5 respectively. Following the principle of building facilities away from active faults, the test system is placed in BSR. It is worth noting that the relative position of EPS buses and NGS nodes are deduced from the length of branches and pipelines respectively, while the gas supply node is located at the same location as the gas power plant.

Assuming that the feasible regions for typhoon basic parameters are divided into 10 segments respectively, while the earthquake magnitude segment interval ΔM is set as 0.5 and the epicentre points are enumerated according to 5 km \times 5 km grids. In this way, a total of 23,806

Table 1 The system-level resilience index under earthquake d_s

Method	r_{sys} (MW)	Error (%)	Time (s)
MCS (Cov = 0.01)	8.325	_	8059.866
MCS (Cov = 0.04)	8.428	1.24	602.279
SE (N-2)	5.586	32.90	46.189
SE (N-3)	7.420	10.87	609.720
IISE (N-2)	8.081	2.93	46.785
IISE (N-3)	8.248	0.92	619.695

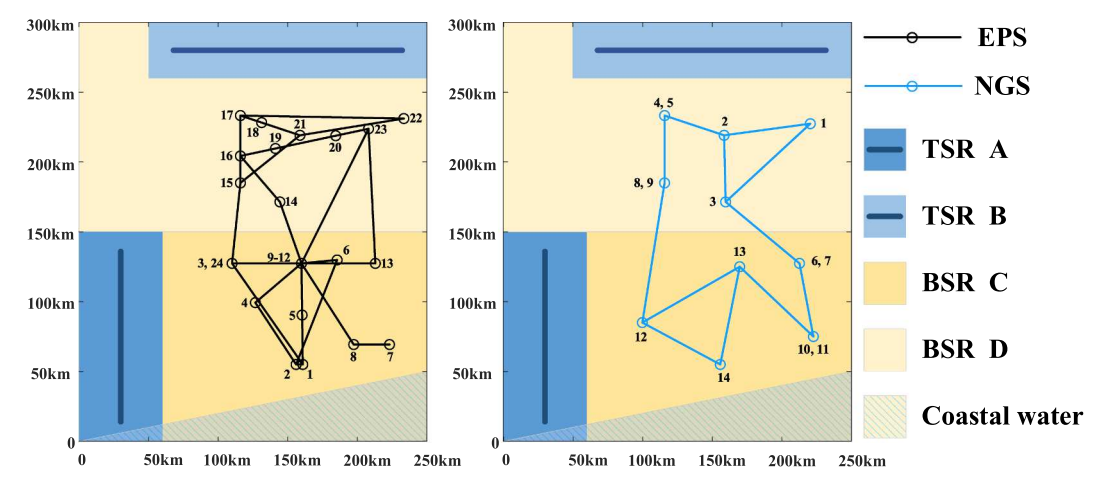


Fig. 13. The spatial location of the test system.

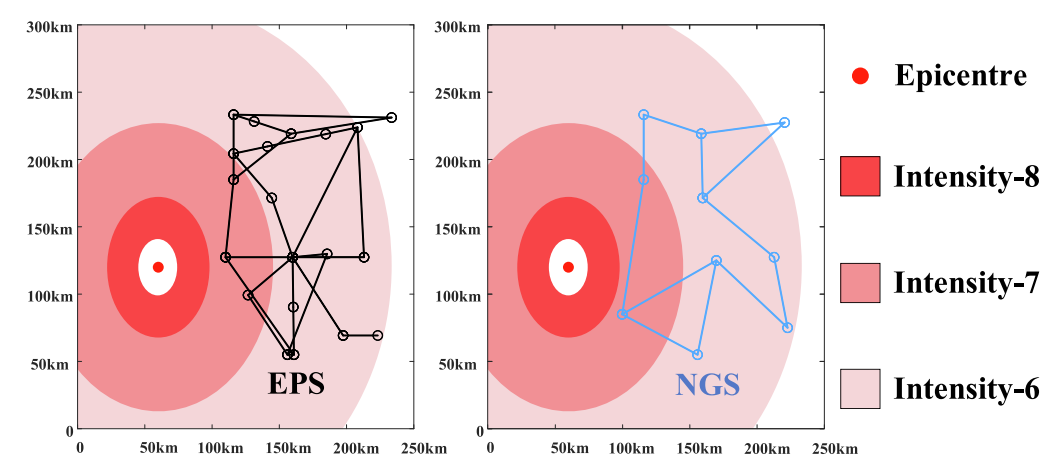


Fig. 14. The earthquake intensity distribution map of d_s .

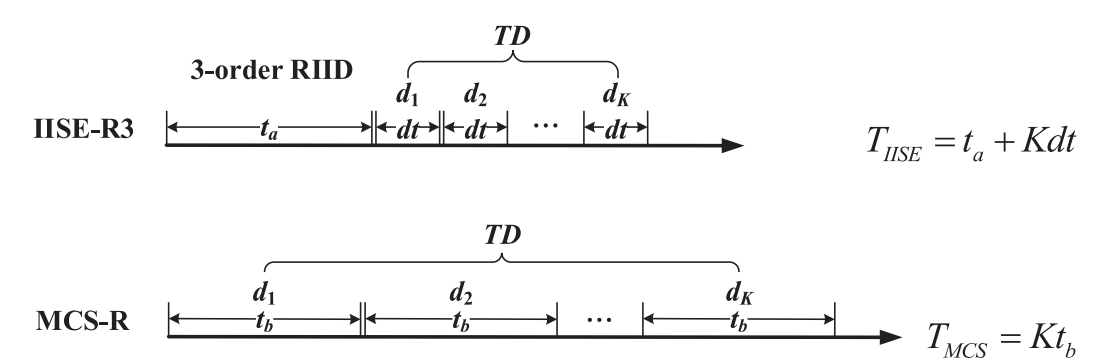


Fig. 15. The comparison of calculation time between IISE-R3 and MCS.

Table 2 The planning-oriented resilience indices based on TD_1 , TD_2 and TD_3 .

TD_1		TD_2		TD_3	
Index	Result (MW)	Index	Result (10 ⁻² MW)	Index	Result (10 ⁻² MW)
R1 sys	1.3436	R2 sys	2.8590	R3 sys	4.7916
R_{27}	0.3366	R_{47}	1.5171	R_{47}	1.4948
R_{10}	0.1791	R_{27}	0.6442	R_{27}	1.1294
R_{11}	0.1785	R_{10}	0.2218	R_{10}	0.4818
R_5	0.1068	R_{46}	0.1695	R_{11}	0.2723
R_{18}	0.0767	R_{48}	0.1508	R_5	0.2638

Table 3The resilience enhancement effects of scheme A, B and C.

Scheme	ΔR1 sys (%)	ΔR2 sys (%)	ΔR3 sys (%)
A	61.06	34.09	45.20
В	38.26	88.97	68.07
C	56.34	86.96	74.34

potential disaster scenarios are enumerated in *TD*, which contains 10,000 typhoon scenarios and 13,806 earthquake scenarios. DSD represents these disaster scenarios with different characteristics in a unified format, which helps to comprehensively analyse the uncertain risks encountered by IEGS.

3.6. Feasibility analysis

The planning-oriented resilience assessment is based on the solutions of r_{sys} and r_n , while Eq. (3) indicates that r_n is solved according to r_{sys} . Therefore, the accuracy and speed of the solving for r_{sys} determine the feasibility of the proposed resilience assessment and enhancement method.

Considering that earthquake disaster affects the components of EPS and NGS at the same time, this paper takes a specific earthquake scenario d_s as a representative disaster scenario. The intensity distribution of d_s is shown in Fig. 14, where the epicentre of d_s is (60, 120), and the earthquake magnitude of d_s belongs to segment $7 \sim 7.5$.

The IISE method is used to solve the system-level resilience index $r_{\rm sys}$ under earthquake $d_{\rm s}$, while the MCS method with the Coefficient of variance (Cov) as 0.04 and the traditional SE method are implemented for comparisons. In addition, the MCS method (Cov = 0.01) is used as a benchmark method. The calculation results are shown in Table. 1, where SE (N-i) and IISE (N-i) represent the SE method and the IISE method that enumerate up to i-order fault states, respectively.

As can be seen from Table 1, the calculation error of IISE method is much less than that of SE method. In addition, the result error of IISE (N-3) is even smaller than that of the MCS (Cov = 0.04) method while having a similar calculation time. During the calculation process of the IISE (N-3) method under earthquake d_{s} , approximately 619.658 s of

619.695 s is spent on solving for the impact-increments which can be invoked from RIID.

In fact, the planning-oriented resilience assessment speed is directly related to the time required to solve set $RD = \{r_{sys,i} | i=1,2,...,K\}$. The method of solving RD based on IISE (N-3) is noted as IISE-R3, while the method of solving RD based on MCS (Cov = 0.04) is noted as MCS-R. Considering that IISE (N-3) method has similar accuracy with MCS (Cov = 0.04) in Table 1, the results of IISE-R3 and MCS-R are also close. Assuming that the calculation time of $r_{sys,i}$ under different disaster scenarios is the same, the total time consumed by IISE-R3 and MCS-R can be estimated according to Table 1.

IISE-R3 method and MCS-R method are compared in Fig. 15, where t_a represents the time consumed for constructing 3-order RIID, dt is the time spent to solve $r_{sys,i}$ using IISE (N-3) with RIID; t_b is the time spent to solve $r_{sys,i}$ using MCS (Cov = 0.04). The parameters in Fig. 15 can take on the following values:

$$\begin{cases}
K = 23806 \\
t_a = 619.658s \\
t_b = 602.279s \\
dt = 619.695 - 619.658 = 0.037
\end{cases} \tag{23}$$

According to Fig. 15 and Eq. (23), the calculation time of IISE-R3 and MCS-R can be estimated as

$$\begin{cases} T_{IISE} \approx 619.658 + 23806 \times 0.037 \approx 1.5 \times 10^{3}(s) \\ T_{MCS} \approx 23806 \times 602.279 \approx 1.434 \times 10^{8}(s) \end{cases}$$
 (24)

 $T_{\it IISE}$ is about one hundred thousandths of $T_{\it MCS}$, which indicates the huge advantage of reusing impact-increments in the IISE method. This highlights the significant advantage of the IISE method over the MCS method in terms of computational efficiency.

Taking both accuracy and speed into account, this paper adopts IISE (*N*-3) to calculate the planning-oriented resilience indices. Based on DSD and 3-order RIID, the proposed resilience assessment and enhancement method can be applied well. It is worth mentioning that the case programs in this paper are implemented on MATLAB R2020b.

3.7. Numerical results

3.7.1. Resilient planning considering the diversity of natural disaster types

To illustrate the necessity of considering multi-type disasters, three
sets of disaster scenarios are proposed as:

- (1) $TD_1 = D_w$, only typhoon is considered.
- (2) $TD_2 = D_e$, only earthquake is considered.
- (3) $TD_3 = D_w \cup D_e$, both typhoon and earthquake are considered.

The IEGS resilience assessment is implemented based on TD_1 , TD_2 and TD_3 respectively. while the system-level resilience indices R1 sys, R2 sys and R3 sys corresponding to these three scenario sets are listed in Table 2. According to the definition of the system-level resilience index, R3 sys is the weighted sum of R1 sys and R2 sys as shown in Eq. (24), while the weight is set based on the annual frequency. Although

typhoons occur less frequently than earthquakes of magnitude 4 or higher, the expected load shedding after one typhoon is greater. Therefore, *R*1 sys is much larger than *R*2 sys and *R*3 sys.

$$R_{sys}^{3} = \frac{f_{w}}{f_{w} + f_{e}} R_{sys}^{1} + \frac{f_{e}}{f_{w} + f_{e}} R_{sys}^{2}$$
 (24)

It is assumed that components are strengthened by increasing redundancy, while at most one spare can be added to each component. In other words, the failure probability of a strengthened component is equal to the square of the initial value. Then, the component-level resilience index R_n of each component can be solved, of which the highest five are listed in Table 2, where the subscript n corresponds to the component number. This paper selects five components for strengthening according to the ranking of R_n , and the resilience enhancement scheme is denoted as the set of components to be enhanced. As shown in Table 2, the resilience enhancement schemes based on TD_1 , TD_2 and TD_3 are scheme A {27, 10, 11, 5, 18}, scheme B {47, 27, 10, 46, 48} and scheme C {47, 27, 10, 11, 5} respectively. It is worth mentioning that the number of each component is given in Appendix C.

The effects of scheme A \sim C are shown in Table 3, where ΔR_{sys} is the percentage of system-level index decline. $\Delta R1$ sys and $\Delta R2$ sys denote the resilience enhancement of IEGS against typhoon and earthquake respectively, while $\Delta R3$ sys denotes the comprehensive resilience improvement of IEGS considering the two types of disasters. When only typhoon disaster is considered, just focus on the column 2 in Table 3: $\Delta R1$ sys of scheme A and scheme C are much higher than scheme B, while $\Delta R1$ sys of scheme A is slightly higher than scheme C. When only earthquake disaster is considered, just focus on the column 3 in Table 3: $\Delta R2$ sys of scheme B and scheme C are much higher than scheme B, while $\Delta R1$ sys of scheme B is slightly higher than scheme C. When both typhoon and earthquake are considered, focus on the column 4 in Table 3: scheme C obtains the highest resilience enhancement $\Delta R3$ sys.

Fig. 16 visualise the resilience enhancement effects of scheme A, B and C. As shown in Fig. 16(a), $\Delta R1$ sys and $\Delta R2$ sys enclose a resilience enhancement rectangle. The length and width of the rectangle corresponding to scheme C are not the biggest among the three schemes, while its area is significantly larger than that of scheme A and scheme B. As Fig. 16(b) shows, scheme C achieves the highest resilience enhancement of IEGS against multi-type disasters.

In a nutshell, scheme A and scheme B provide the greatest increase in system resilience to a single type of disaster, but less to another disaster types. By contrast, Scheme C takes the diversity of disaster types into account and can comprehensively improve the resilience of IEGS considering multi-type disasters.

3.7.2. Resilient planning considering the economic factor

The resilience enhancement scheme according to the component-level index R_n provides the greatest increase in resilience, while the scheme according to the economic index C_n pursues the most cost-effective resilience enhancement.

Assuming that the cost of each transformer is 0.6 million USD, the cost of overhead transmission line and gas pipeline are 1 million USD/km and 2 million USD/km respectively. The top five components with the smallest C_n are given in Table 4, while the top five components with the largest R_n are listed for comparison. It is worth noting that the set of disaster scenarios considered below is TD_3 .

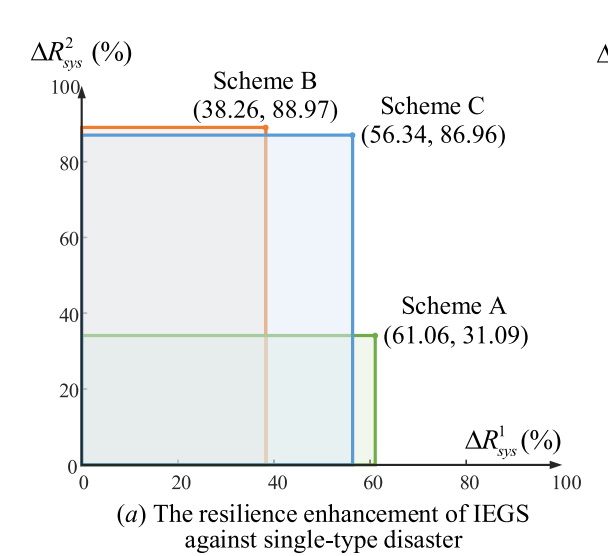
 C_n is ranked from small to large according to the cost-effectiveness ratio of strengthening each component, and the ranking result is different from R_n . For example, component 47 is ranked first in R_n , while its C_n is ranked fifth. This is because, although reinforcing component 47 is quite effective, the high cost of reinforcement pulls down the cost-effectiveness ratio. The resilience enhancement scheme according to the ranking of C_n is denoted as scheme D {27, 10, 7, 11, 47}. It can be seen from Table 5 that scheme D possesses a slightly lower resilience enhancement effect than the scheme C, while it is much more cost-effective. When sufficient funds are available, scheme C is undoubtedly the best choice. However, scheme D is more suitable with insufficient budget, as it balances the resilience enhancement effect with the implementation cost.

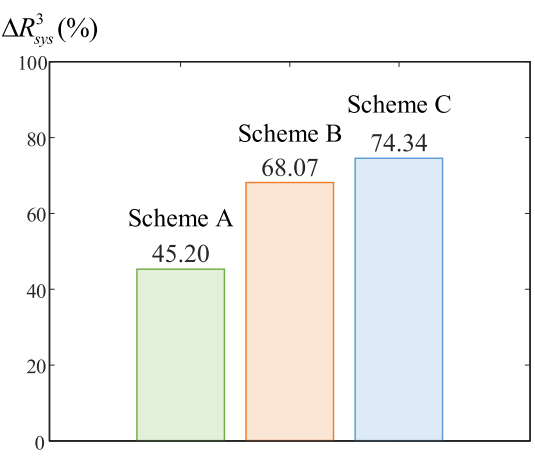
Table 4 The economic index C_m and the component-level index R_n .

Number	C_n (billion USD/MW)	Number	$R_n (10^{-2} \text{MW})$
27	5.1299	47	1.4948
10	5.3445	27	1.1294
7	7.9641	10	0.4818
11	9.4574	11	0.2723
47	9.7490	5	0.2638

Table 5 The scheme C according to R_n versus the scheme D according to C_n

Scheme	ΔR_{sys} (%)	Cost (billion USD)	Cost/ ΔR_{sys}
С	74.34	0.3356	0.0451
D	70.33	0.2558	0.0364





(b) The resilience enhancement of IEGS against multi-type disasters

Fig. 16. The resilience enhancement comparison of scheme A, B and C.

4. Conclusion and future work

This paper proposes a resilience assessment and enhancement method for IEGS considering multi-type potential disasters within planning time scale. The disaster scenario database (DSD) has been developed to fully represent the impact of all potential disasters during the planning period. The reusable impact-increment database (RIID) is constructed, and the planning-oriented indices are calculated by repeatedly invoking RIID. Component-level indices are calculated to locate the weak points of the IEGS, and enhancement strategies are developed accordingly. Resilience assessment of a test IEGS system in Taiwan coastal seismic statistical zone confirms that IISE owns a fairly high calculation accuracy. The comparison results between the IISE-R3 and MCS (COV = 0.04) demonstrate the advantage of using RIID to improve computational efficiency. The resilience assessment results indicate the importance of considering the diversity of disaster types and the necessity to concern the economic factor under insufficient budget.

The proposed resilience enhancement scheme strengthens the top five components based on the ranking of resilience indices, while the logic of the strengthening order fails to be reflected. As for the background of resilience enhancement, the budgetary cost limitation is not considered in this paper, as well as the requirement for system-level resilience indices to meet the standard. These issues will be studied in our future work. Besides, this paper analyses the robustness and the redundancy of resilience for IEGS in a targeted manner, while other resilience factors can be studied in depth later. For example, the rapidity

can be considered by adding the weighted post-disaster recovery time to resilience indices, and the resourcefulness can be considered by configuring resources on standby that can be quickly allocated to an area of need.

CRediT authorship contribution statement

Han Wang: Conceptualization, Methodology, Software, Writing – original draft. Kai Hou: Conceptualization, Supervision, Writing – review & editing, Project administration. Junbo Zhao: Validation, Writing – review & editing. Xiaodan Yu: Supervision, Writing – review & editing. Hongjie Jia: Supervision, Writing – review & editing. Yunfei Mu: Software, Validation.

Declaration of Competing Interest

The authors declare that they have no known competing financial interests or personal relationships that could have appeared to influence the work reported in this paper.

Acknowledgements

This work was supported by the joint project of NSFC of China and EPSRC of UK (No.52061635103 and EP/T021969/1) and the National Natural Science Foundation of China (Grant No. 52077150).

Appendix A. . Proof of the necessity to modify the Component-Level index

According to Eq. (7), the system-level resilience index r_{sys} is obtained by

$$r_{sys} = \sum_{i=1}^{J} \sum_{s \in \Omega_i} (\prod_{i \in s} p_i) \Delta I_s \tag{A.1}$$

Substitute Eq. (A.1) into Eq. (3), thus expressing resilience indices r'_n and r_n as

$$\begin{cases} r_{n}^{'} = p_{n} \frac{\partial r_{sys}}{\partial p_{n}} + r_{n} = (p_{n} - p_{n}^{'}) \frac{\partial r_{sys}}{\partial p_{n}} \\ \frac{\partial r_{sys}}{\partial p_{n}} = \sum_{j=1}^{J} \sum_{s \in \Omega_{j}} (\prod_{i \in s} p_{i}) \Delta I_{s} \\ r \in s \quad i \neq n \end{cases}$$
(A.2)

where $\frac{\partial r_{sys}}{\partial p_n}$ is the partial derivative of r_{sys} with respect to p_n , while its expression does not include p_n .

Set the ratio of r_n to r_n as η , which is expressed as

$$\eta = \frac{r'_n}{r_n} = \frac{p_n}{p_n - p'_n} \tag{A.3}$$

Obviously, η is constant only when the strengthening measure reduces p_n proportionately, which means that the component ranking based on r'_n may be different from the ranking based on r_n . Therefore, it's necessary to modify the definition of the component-level index so that the effect of strengthening measure is accurately described.

Appendix B

Typhoon modelling

As shown in Table B1, the basic typhoon parameters include typhoon landing site (x_0,y_0), typhoon direction angle θ , original central pressure difference ΔH_0 (hPa) and typhoon moving speed (km/h), while the direct typhoon parameter is the real-time speed v(t) at each point in the wind farm.

Typhoon probability model

According to Ref. [11], the typhoon landing site is supposed to obey a uniform probability distribution along the coastline, while the motion direction obeys a binormal probability distribution. In addition, the original pressure difference and translational speed obey the lognormal probability distribution.

Table B1Potential natural disaster types.

Disaster Type	Basic parameters	Direct parameters
Wildfire Flood	Fire-starting pointWildfire intensityWind speedWind direction Rainfall intensityPrecipitation	The density, temperature, humidity,pressure and soot concentration of air Runoff distribution

After determining the feasible region of each typhoon basic parameter, the set of potential typhoon scenarios can be obtained by applying the combinatorial enumeration method with reference to Fig. 5. For the potential typhoon scenario d_w , the occurrence probabilities of its landing site ($x_{0,w}$, $y_{0,w}$), motion direction θ_w , original pressure difference $\Delta H_{0,w}$ and translational speed $v_{T,w}$ are expressed as

$$\begin{cases} P_{r}(x_{0,w}, y_{0,w}) = \frac{ds}{s} \\ P_{r}(\theta_{w}) = \int_{\theta_{w} - \frac{d\theta}{2}}^{\theta_{w} + \frac{d\theta}{2}} \frac{1}{\sqrt{2\pi}} \left[\frac{\varepsilon}{\sigma_{l}} e^{-\frac{(x-\mu_{l})^{2}}{2\sigma_{l}^{2}}} + \frac{1-\varepsilon}{\sigma_{2}} e^{-\frac{(x-\mu_{l})^{2}}{2\sigma_{2}^{2}}} \right] dx \\ P_{r}(\Delta H_{0,w}) = \int_{\ln(\Delta H_{0,w} - \frac{d\theta}{2})}^{\ln(\Delta H_{0,w} + \frac{d\theta}{2})} \frac{1}{\sqrt{2\pi} \sigma_{H}} e^{-\frac{(x-\mu_{H})^{2}}{2\sigma_{H}^{2}}} dx \\ P_{r}(v_{T,w}) = \int_{\ln(v_{T,w} - \frac{d\theta}{2})}^{\ln(v_{T,w} + \frac{d\theta}{2})} \frac{1}{\sqrt{2\pi} \sigma_{v}} e^{-\frac{(x-\mu_{v})^{2}}{2\sigma_{v}^{2}}} dx \end{cases}$$

$$(B.1)$$

where *S* is the length of the coastline; ds, $d\theta$, dH, dv are the segment intervals of the feasible regions of typhoon basic parameters; μ_1 , σ_1 , μ_2 , σ_2 , ε , μ_H , σ_H , μ_V , σ_V are the distribution parameters.

As shown in Fig. B1, the occurrence probability of typhoon d_w can be obtained by

$$P_{w} = P_{r}(x_{0,w}, y_{0,w}) P_{r}(\theta_{w}) P_{r}(\Delta H_{0,w}) P_{r}(v_{T,w})$$
(B.2)

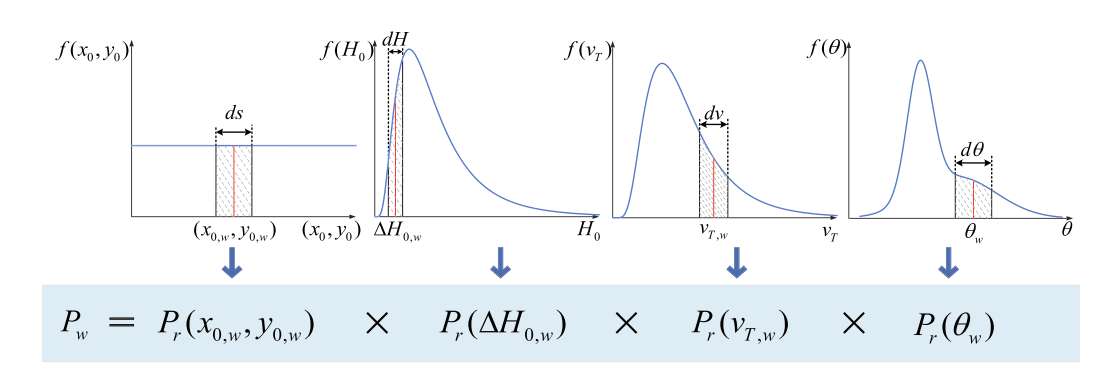


Fig. B1. The occurrence probability of the generated typhoon scenario.

Typhoon attack model

Taking the typhoon landing as the initial moment, the real-time wind speed directly related to the component failure probability can be obtained by [29]

$$\Delta H(t) = \Delta H_0 - 0.677[1 + \sin(\xi - \theta)]t \tag{B.3}$$

$$r_{max}(t) = 1.119 \times 10^3 \Delta H(t)^{-0.805}$$
 (B.4)

$$v_{rmax}(t) = 5.221\sqrt{\Delta H(t)} + 0.1389v_T$$
 (B.5)

$$v_d(t) = \begin{cases} v_{max}(t)[d(t)/r_{max}(t)], d(t) \leq r_{max}(t) \\ v_{max}(t)[r_{max}(t)/d(t)], d(t) > r_{max}(t) \end{cases}$$
(B.6)

$$T = min\{\frac{\Delta H_0}{0.677[1 + sin(\xi - \theta)]}, 240\}$$
(B.7)

where $\Delta H(t)$ is the central pressure difference at time t (hour); ξ is the clockwise angle between the coastline and the due north direction; $r_{max}(t)$ is the maximum wind speed radius at time t; $v_{rmax}(t)$ (m/s) is the maximum wind speed at time t, $v_d(t)$ is the real-time wind speed at the point with distance d(t) from the typhoon centre at time t; T is the typhoon duration, of which the upper limit is set to 240 h.

As shown in Fig. B2, typhoon lands on coastline and travels toward hinterland along the angle θ with speed v_T . According to Eq. (B.6), the real-time wind speed at (x_d, y_d) is $v_{rmax}(t_1)[r_{max}(t_1)/d(t_1)]$ at time t_1 and $v_{rmax}(t_2)[d(t_2)/r_{max}(t_2)]$ at time t_2 .

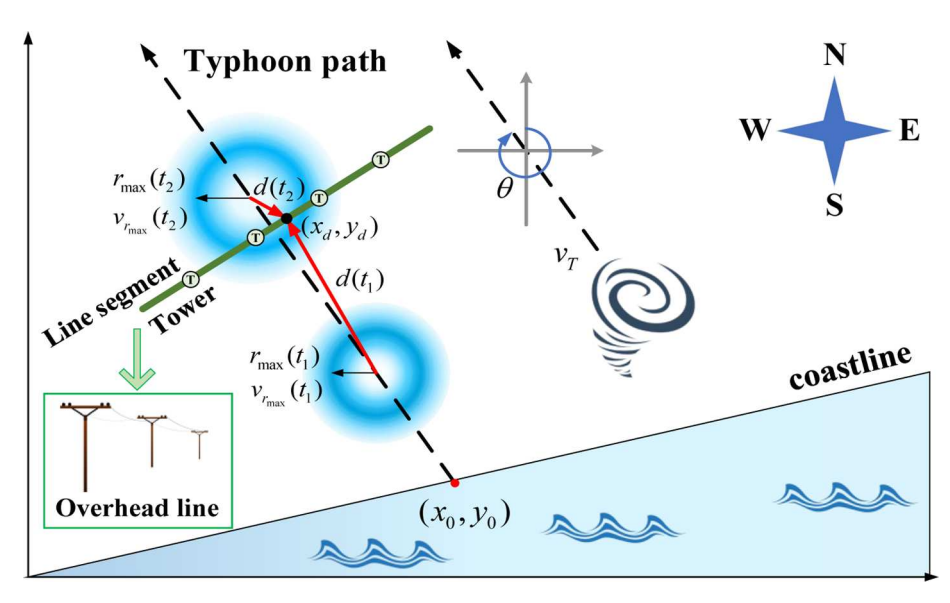


Fig. B2. Typhoon path diagram.

It is difficult for the typhoon to pose a substantial threat to transformers and NGS components [30]. Therefore, this paper assumes that typhoons only cause damage to the overhead line. Component failure probability is related to the real-time wind speed at the point where the component is located, while the position of the line segment is taken as its midpoint. The failure probabilities of the tower and the line segment at time t are expressed as [11]

$$\delta_h(t) = \begin{cases} 0, & v_h(t) \in [0, v_{d,hv}] \\ e^{y[v_h(t) - 2v_{d,tw}]}, & v_h(t) \in [v_{d,tw}, 2v_{d,tw}] \\ 1, & v_h(t) \in [2v_{d,tw}, \infty] \end{cases}$$
(B.8)

$$\delta_{h'}(t) = exp[11 \times \frac{v_{h'}(t)}{v_{d,ls}} - 18]\Delta h$$
 (B.9)

where $v_h(t)$ and $v_{h'}(t)$ are the real-time wind speeds of tower h and line segment h' respectively; $v_{d,tw}$ and $v_{d,ls}$ are respectively the design wind speeds of tower and line segment; γ is the model coefficient, which is taken as 0.4 in this paper; Δh (km) is the length of the line segment.

The cumulative failure probabilities of the tower h and the line segment h' during the typhoon are obtained by [11]

$$\begin{cases} \lambda_{h} = 1 - exp\{-\sum_{k=0}^{N_{t}-1} [\delta_{h}(k\Delta t)/(1 - \delta_{h}(k\Delta t))]\Delta t\} \\ \lambda_{h'} = 1 - exp[-\sum_{k=0}^{N_{t}-1} \delta_{h'}(k\Delta t)\Delta t] \end{cases}$$
(B.10)

where N_t is the number of time segments; Δt is the interval of each time segment, which is taken as 1 h.

The towers and line segments of the same overhead line form a series system, so the failure probability of overhead line ω is obtained by

$$p_{\omega} = 1 - \prod_{h \in \omega} (1 - \lambda_h) \prod_{h' \in \omega} (1 - \lambda_{h'})$$
(B.11)

List of other potential disaster types

In DPM of wildfire disaster, the distribution functions of the fire-starting point, wildfire intensity, wind speed and wind direction can be obtained by the multivariate logistic regression model. DAM of wildfire disaster applies the wildfire spread model to get the air physicochemical properties of each point in the affected area, so as to calculate the component failure probability under wildfire condition. For example, the failure probability of transmission line is related to the breakdown voltage of air gaps, which can be solved based on the wildfire direct parameters.

Suppose that the flood disaster is caused by rainfall. DPM of flood disaster obtains the distribution of rainfall intensity and precipitation based on historical statistical data, which can be used to generate potential floods. In DAM of flood disaster, Xinanjiang model [31] can be used to calculate the runoff distribution, which is used as input to the component probability model.

The proposed unified research framework still applies to wildfire and flood. However, for some uncommon types of disaster, the associated modelling is extremely difficult and their incorporation into DSD still requires breakthroughs in the relevant fields.

Appendix C. . Detailed introduction of the test system

The EPS parameters in the test system is given in Ref. [32], while component number $1 \sim 38$ correspond to the rows of the IEEE RTS 79 branch matrix in order. Therefore, the NGS component number starts from 39 as shown in Table C3.

The parameters of the four gas power plants are listed in Table C1, where P_{max} and P_{min} are the upper and lower limits of the output of gas power

Table C1Gas power plant parameters.

EPS Bus	NGS Node	P_{max} (MW)	P _{min} (MW)	a (Sm ³ /MWh)
2	14	192	0	180
13	7	591	0	180
15	8	215	0	180
21	2	400	0	180

plants respectively; a represents the natural gas required per 1MWh of electricity output.

The natural gas system node parameters are listed in Table C2, where G_d is the gas load and G(P) means that the gas load of the node depends on the output of the gas power plant connected to it; S_{max} and S_{min} are the upper and lower limits of the gas source output respectively; π_{max} and π_{min} are the upper and lower limits of the nodal pressure respectively.

Table C2Natural gas system node parameters.

Node	G _d (MMCFD)	S _{max} (MMCFD)	S_{\min} (MMCFD)	π_{max} (psia)	π_{min} (psia)
1	_	250	0	1200	600
2	G(P)	_	_	700	400
3	40	_	_	700	400
4	0	_	_	1200	600
5	0	_	_	1200	600
6	0	_	_	1200	600
7	G(P)	-	_	700	400
8	G(P)	-	_	700	400
9	0	_	_	1200	600
10	_	250	0	1200	600
11	0	_	_	1200	600
12	50	_	_	700	400
13	50	_	_	700	400
14	G(P)	_	_	700	400

Table C3Natural gas system pipeline parameters.

Number	From	То	L (km)	K (MMCFD/psia)
39	Node 1	Node 2	62.5634	0.3635
40	Node 1	Node 3	82.7830	0.3158
41	Node 2	Node 3	47.7344	0.4105
42	Node 2	Node 4	45.0616	0.4319
43	Node 3	Node 6	68.9798	0.3495
44	Node 5	Node 8	48.2803	0.4175
45	Node 7	Node 10	53.3592	0.2577
46	Node 9	Node 12	101.3107	0.1766
47	Node 11	Node 13	72.8629	0.2080
48	Node 12	Node 13	80.6226	0.2101
49	Node 12	Node 14	63.5522	0.2365
50	Node 13	Node 14	71.3812	0.2105

The natural gas system pipeline parameters are listed in Table C1, where L is the length of the pipeline; K is the parameter in Weymouth equation, which is expressed as

$$f^2 = K^2 \left| \pi_{From}^2 - \pi_{To}^2 \right| \tag{C.1}$$

where f is the gas flow in the pipeline, π_{From} and π_{To} are the inlet and outlet pressures of the pipeline respectively.

The natural gas compressor parameters are listed in Table C4, where k_{max} and k_{min} are the upper and lower limits of the compression ratio kc respectively; D_c is the parameter in the consumption characteristic equation, which is expressed as

$$G_c = D_c f_c \left(k_c^{\frac{a-1}{a}} - 1 \right) \tag{C.2}$$

where G_c is the gas consumption of the compressor; f_c is the gas flow through the compressor; α is the polytropic index of compression, which is taken as 1.4.

Table C4Natural gas compressor parameters.

From	То	k _{max}	k_{min}	D_c
Node 4	Node 5	1.8	1.2	0.0129
Node 6	Node 7	1.8	1.2	0.0129
Node 8	Node 9	1.8	1.2	0.0129
Node 10	Node 11	1.8	1.2	0.0129

Appendix D. . Disaster modelling parameters

Ref. [11] provides the distribution of typhoon basic parameters, which are listed in Table D1.

To reflect a certain level of typhoon resistance for the overhead transmission line, the design wind speeds of the tower and transmission line segments are both set as 35 m/s.

Considering that the test system is in Taiwan seismic statistical area, the G-R coefficient b is taken as 0.92. In addition, the earthquake intensity attenuation parameters sourced from Ref. [34–35] are shown in Table D2 and Table D3 respectively.

Table D1The distributions of the typhoon basic parameters in the study area.

		•
Typhoon Basic Parameter	Feasible Region	Distribution Expression
(x_0,y_0)	(0,0)~(0,250)	$\begin{cases} x_0 \tilde{\mathbf{U}}(0, 250) \\ y_0 = x_0 / 5 \end{cases}$
θ	$-180^{\circ}{\sim}180^{\circ}$	$\theta \widetilde{S(-73.3392,22.5891^2;-7.2084,70.3532^2;0.5035)}$
ΔH_0	$0\sim 80\;hPa$	$ln\Delta H_0 \tilde{N}(2.9001, 0.6274^2)$
$ u_T$	$0\sim 50\; km/h$	$\textit{lnv}_{T}\tilde{N}(2.6680, 0.5185^{2})$

Table D2The earthquake intensity attenuation parameters.

Intensity attenuation parameter	value
long axis A_1 /short axis A_2	5.7123 / 3.6588
long axis B_1 /short axis B_2	1.3626 / 1.3626
long axis C_1 /short axis C_2	-4.2903 / -3.5406
long axis ϕ_1 /short axis ϕ_2	25 km / 13 km

Table D3Parameters related to component failure probability under earthquake.

Parameter	Intensity-6	Intensity-7	Intensity-8
$p_{ au}$	2.55E-06	7.03E-06	1.83E-04
λ_a	6.45E-06	5.04E-04	2.57E-03
R_f	0.0001	0.001	0.01

References

- [1] T. Adachi, Y. Ishiyama, Y. Asakura, K. Nakamura. The restoration of telecom power damages by the Great East Japan Earthquake. 2011 IEEE 33rd International Telecommunications Energy Conference (INTELEC), 2011;1-5.
- [2] Lanzano G, Santucci de Magistris F, Fabbrocino G, Salzano E. Seismic damage to pipelines in the framework of Na-Tech risk assessment. J Loss Prev Process Ind 2015;33:159, 72
- [3] T. Li, B. Luo, L. Liu, T. Wu. Wind accident analysis of transmission line in China Southern Power Grid's Coastal Regions. 2015 5th International Conference on Electric Utility Deregulation and Restructuring and Power Technologies (DRPT), 2015: 1700-1704.
- [4] Panteli M, Pickering C, Wilkinson S, Dawson R, Mancarella P. Power System Resilience to Extreme Weather: Fragility Modeling, Probabilistic Impact Assessment, and Adaptation Measures. IEEE Trans Power Syst 2017;32(5): 3747–57.
- [5] Jufri FH, Widiputra V, Jung J. State-of-the-art review on power grid resilience to extreme weather events: Definitions, frameworks, quantitative assessment methodologies, and enhancement strategies. Appl Energy 2019;239:1049–65.
- [6] Schlör H, Venghaus S, Hake J-F. The FEW-Nexus city index Measuring urban resilience. Appl Energy 2018;210:382–92.

- [7] Hossain E, Roy S, Mohammad N, Nawar N, Dipta DR. Metrics and enhancement strategies for grid resilience and reliability during natural disasters. Appl Energy 2021;290:116709. https://doi.org/10.1016/j.apenergy.2021.116709.
- [8] Ouyang M, Dueñas-Osorio L. Multi-dimensional hurricane resilience assessment of electric power systems. Struct Saf 2014;48:15–24.
- [9] ZOBEL C W. Comparative visualization of predicted disaster resilience. Proceedings of the 7th International ISCRAM Conference, May 2-5, 2010, Seattle, USA: 1-6.
- [10] Panteli M, Mancarella P, Trakas DN, Kyriakides E, Hatziargyriou ND. Metrics and Quantification of Operational and Infrastructure Resilience in Power Systems. IEEE Trans Power Syst 2017;32(6):4732–42.
- [11] Liu X, Hou K, Jia H, Zhao J, Mili L, Jin X, et al. A Planning-oriented Resilience Assessment Framework for Transmission Systems under Typhoon Disasters. IEEE Trans. Smart Grid 2020;11(6):5431–41.
- [12] Zheng Y, Wu J, Fu J, et al. The Resilience Assessment Method of Electric-gas System under Earthquake Disaster. In: 2020 IEEE 3rd Student Conference on Electrical Machines and Systems (SCEMS); 2020. p. 591–5.
- [13] Shao C, Shahidehpour M, Wang X, Wang X, Wang B. Integrated Planning of Electricity and Natural Gas Transportation Systems for Enhancing the Power Grid Resilience. IEEE Trans Power Syst 2017;32(6):4418–29.
- [14] Hou K, Jia H, Xiaodan Yu, Zhu L, Xiandong Xu, Li X. An impact increments-based state enumeration reliability assessment approach and its application in transmission systems. IEEE Power and Energy Society General Meeting (PESGM) 2016;2016:1–5.

- [15] Aldarajee AHM, Hosseinian SH, Vahidi B, Dehghan S. A coordinated planner-disaster-risk-averse-planner investment model for enhancing the resilience of integrated electric power and natural gas networks. Int J Electr Power Energy Syst 2020;119:105948. https://doi.org/10.1016/j.ijepes.2020.105948.
- [16] Lin Y, Bie Z. Tri-level optimal hardening plan for a resilient distribution system considering reconfiguration and DG islanding. Appl Energy 2018;210:1266–79.
- [17] Sayed AR, Wang C, Bi T. Resilient operational strategies for power systems considering the interactions with natural gas systems. Appl Energy 2019;241: 548–66
- [18] Li G, Zhang P, Luh PB, Li W, Bie Z, Serna C, et al. Risk Analysis for Distribution Systems in the Northeast U.S. Under Wind Storms. IEEE Trans Power Syst 2014;29 (2):889–98
- [19] Kusumastuti RD, Viverita, Husodo ZA, Suardi L, Danarsari DN. Developing a resilience index towards natural disasters in Indonesia. Int J Disaster Risk Reduct 2014;10(Part A):327–40.
- [20] Lee C-H, Lin S-H, Kao C-L, Hong M-Y, Huang P-C, Shih C-L, et al. Impact of climate change on disaster events in metropolitan cities -trend of disasters reported by Taiwan national medical response and preparedness system. Environ Res 2020; 183:109186. https://doi.org/10.1016/j.envres.2020.109186.
- [21] Liu X, Hou K, Jia H, Zhao J, Mili L, Mu Y, et al. A resilience assessment approach for power system from perspectives of system and component levels. Int J Electr Power Energy Syst 2020;118:105837. https://doi.org/10.1016/j. ijenes.2020.105837.
- [22] H. Wang, K. Hou, X. Yu, H. Jia. (2021, Apr.). The Assessment and Improvement Method of Electricity-gas System Resilience Considering Earthquake Disaster Uncertainty. *Proceedings of the CSEE*. [Online]. Available: https://doi.org/ 10.13334/j. 0258-8013. pcsee.202243 (in Chinese).
- [23] Seismic ground motion parameters zonation map of China, GB 18306-2015.
- [24] Gutenberg B, Richter CF. Frequency of earthquakes in California. Bull Seismol Soc Am 1994;34(4):185–8.

- [25] Zhang Y, Weng WG, Huang ZL. A scenario-based model for earthquake emergency management effectiveness evaluation. Technol Forecast Soc Chang 2018;128 (Mars.):197–207.
- [26] Cimellaro GP, Villa O, Bruneau M. Resilience-Based Design of Natural Gas Distribution Networks. J Infrastruct Syst 2015;21(1):05014005. https://doi.org/ 10.1061/(ASCE)IS.1943-555X.0000204.
- [27] Podimata M. Methodological approach to EIA due to gas pipeline failure after an earthquake. The case study of the Trans Adriatic Pipeline. J Nat Gas Sci Eng 2016; 35:1200–6.
- [28] Ma Q, Li S, Li S, Tao D. On the correlation of ground motion parameters with seismic intensity. Earthquake Engineering and Engineering Dynamics 2014;34(04): 83–92. in Chinese.
- [29] Batts ME, Simiu E, Russell LR. Hurricane wind speeds in the United States. J. Struct. Division 1980;106(10):2001–16.
- [30] Zhang H, Wang P, Yao S, Liu X, Zhao T. Resilience Assessment of Interdependent Energy Systems Under Hurricanes. IEEE Trans Power Syst 2020;35(5):3682–94.
- [31] Ren-Jun Z. The Xinanjiang Model Applied in China. J Hydrol 1992;135(1-4):
- [32] Subcommittee P. IEEE reliability test system. IEEE Transactions on Power Apparatus and Systems 1979;PAS-98(6):2047–54.
- [33] Y. Yu, S. Li, L. Xiao. Development of Ground Motion Attenuation Relations for the New Seismic Hazard Map of China. Technology for Earthquake Disaster Prevention, 2013, 8(01): 24-33 (in Chinese).
- [34] He H, Guo J. Components Damage Probability Analysis of Power System Based on Seismic Zonation. Power System Technology 2011;35(012):38–42. in Chinese.
- [35] Kim K, Ren A. Analysis of earthquake damage ratio of buried gas pipe. Journal of Natural Disasters 2007;16(3):148–53. in Chinese.
- [36] Liu Zeyu, Hou Kai, Jia Hongjie, et al. A Lagrange Multiplier Based State Enumeration Reliability Assessment for Power Systems with Multiple Types of Loads and Renewable Generations. IEEE Transactions on Power Systems 2021;36 (4):3260–70.